

THE EFFECT OF PECULIAR VELOCITIES ON SUPERNOVA COSMOLOGY

TAMARA M DAVIS,^{1,2} LAM HUI,³ JOSHUA A. FRIEMAN,^{4,5,6} TROELS HAUGBØLLE,⁷ RICHARD KESSLER,^{5,4}
BENJAMIN SINCLAIR,¹ JESPER SOLLERMAN,^{7,8} BRUCE BASSETT,^{9,10} JOHN MARRINER,⁶ EDVARD MÖRTSELL,¹¹
ROBERT C. NICHOL,¹² MICHAEL W. RICHMOND,¹³ MASAO SAKO,¹⁴ DONALD P. SCHNEIDER¹⁵*Draft version March 16, 2019*

ABSTRACT

We present an analysis of peculiar velocities and their effect on supernova cosmology. In particular, we study (a) the corrections due to our own motion, (b) the effects of correlations in peculiar velocities induced by large-scale structure, and (c) uncertainties arising from a possible local under- or over-density. For all of these effects we present a case study of their impact on the cosmology derived by the Sloan Digital Sky Survey-II Supernova Survey (SDSS-II SN Survey).

Correcting supernova redshifts for the CMB dipole slightly over-corrects nearby supernovae that share some of our local motion. We show that while neglecting the CMB dipole would cause a shift in the derived equation of state of $\Delta w \sim 0.04$ (at fixed Ω_m) the additional local-motion correction is currently negligible ($\Delta w \lesssim 0.01$).

We use a covariance-matrix approach to statistically account for correlated peculiar velocities. This down-weights nearby supernovae and effectively acts as a graduated version of the usual sharp low-redshift cut. Neglecting coherent velocities in the current sample causes a systematic shift of $\sim 2\%$ in the preferred value of w and will therefore have to be considered carefully when future surveys aim for percent-level accuracy.

Finally, we perform n -body simulations to estimate the likely magnitude of any local density fluctuation (monopole) and estimate the impact as a function of the low-redshift cutoff. We see that for this aspect the low- z cutoff of $z = 0.02$ is well-justified theoretically, but that living in a putative local density fluctuation leaves an indelible imprint on the magnitude-redshift relation.

Subject headings: cosmology: observations — supernovae : general

1. INTRODUCTION

tamarad@physics.uq.edu.au

¹ School of Mathematics and Physics, University of Queensland, QLD, 4072, Australia

² Dark Cosmology Centre, Niels Bohr Institute, University of Copenhagen, Juliane Maries Vej 30, DK-2100 Copenhagen Ø, Denmark

³ Department of Physics, Institute for Strings, Cosmology and Astroparticle Physics (ISCAP), Columbia University, New York, NY 10027

⁴ Kavli Institute for Cosmological Physics, The University of Chicago, 5640 South Ellis Avenue Chicago, IL 60637

⁵ Department of Astronomy and Astrophysics, The University of Chicago, 5640 South Ellis Avenue, Chicago, IL 60637

⁶ Center for Particle Astrophysics, Fermi National Accelerator Laboratory, P.O. Box 500, Batavia, IL 60510

⁷ Niels Bohr Institute, University of Copenhagen, Juliane Maries Vej 30, DK-2100 Copenhagen Ø, Denmark

⁸ The Oskar Klein Centre, Department of Astronomy, AlbaNova, Stockholm University, SE-106 91 Stockholm, Sweden

⁹ Department of Mathematics and Applied Mathematics, University of Cape Town, Rondebosch 7701, South Africa

¹⁰ South African Astronomical Observatory, P.O. Box 9, Observatory 7935, South Africa.

¹¹ Department of Physics, AlbaNova, Stockholm University, SE-106 91 Stockholm Sweden

¹² Institute of Cosmology and Gravitation, Dennis Sciama Building, Burnaby Road, University of Portsmouth, Portsmouth, PO1 3FX, UK

¹³ Physics Department, Rochester Institute of Technology, 85 Lomb Memorial Drive, Rochester, NY 14623-5603

¹⁴ Department of Physics and Astronomy, University of Pennsylvania, Philadelphia, PA 19104

¹⁵ Department of Astronomy and Astrophysics, The Pennsylvania State University, 525 Davey Laboratory, University Park, PA 16802.

The picture of our universe that comes out of observations of supernovae, the cosmic microwave background, and baryon acoustic oscillations (amongst other tests) is of an on-average homogeneous, isotropic universe primarily composed of around 30% matter and 70% dark energy, where the dark energy properties are consistent with a cosmological constant (Riess et al. 1998; Perlmutter et al. 1999; Page et al. 2003; Eisenstein et al. 2005; Tegmark et al. 2006; Spergel et al. 2006; Astier et al. 2006; Wood-Vasey et al. 2007; Riess et al. 2004, 2007; Kowalski et al. 2008; Hicken et al. 2009; Kessler et al. 2009; Percival et al. 2007, 2010; Freedman et al. 2009; Komatsu et al. 2009, 2010). This is known as the concordance cosmology, or Λ CDM. The homogeneous and isotropic part of the concordance cosmology is an assumption we impose on the data before we calculate the densities of matter and dark energy. Large scale structure surveys and the isotropy of the cosmic microwave background provide strong evidence that such an assumption is justified on scales larger than galaxy superclusters (~ 100 Mpc). On smaller scales it is clear that the assumption is a phenomenally poor one.

Whether the local inhomogeneities are significant enough to bias our inferences from cosmological observations is a pertinent question as we strive to make ever more precise measurements of cosmological features, such as the equation of state of dark energy, and as we endeavour to use cosmology to constrain other fundamental physics, such as the neutrino mass.

Type Ia supernovae (SNe Ia) have now become a stan-

dard tool in cosmology (Schmidt et al. 1998; Riess et al. 1998; Perlmutter et al. 1999; Perlmutter & Schmidt 2003; Astier et al. 2006; Wood-Vasey et al. 2007; Kowalski et al. 2008; Kessler et al. 2009). The customary diagnostic is the Hubble diagram, a measurement of luminosity as a function of redshift. To date, the majority of the effort in calibrating supernova measurements has been increasing the accuracy and precision with which we can determine their luminosity, and thus their use as a standard candle. In comparison the uncertainty on the redshift of the supernovae has usually been considered negligible. It is this more neglected uncertainty we turn our attention to in this study.

As supernova measurements become increasingly precise, and the increasing number of supernovae reduces the statistical uncertainty, it is worth revisiting the redshift uncertainty to ensure that it does not bias our cosmological results. The measurement of redshift will remain far more accurate than the measurement of the supernova magnitude into the foreseeable future. However, the accuracy of those measurements can be misleading since systematic effects on redshift due to peculiar motions can be much larger than the measurement error (see Fig. 1).

In a statistical sense peculiar velocities can be used as a signal to detect large scale structure by its gravitational influence and thus measure cosmological parameters using diagnostics such as the peculiar velocity power spectrum (e.g. Bonvin et al. 2006a; Neill et al. 2007; Gordon et al. 2007, 2008; Abate & Lahav 2008; Hannestad et al. 2008). In Lampeitl et al. (2010, App. B) we showed that the signal in the SDSS SN data set is too small to measure cosmological parameters this way (mostly because our sample is too distant). Here we therefore concentrate only on the deleterious impact peculiar velocities have on the cosmological results derived from the SN magnitude-redshift relation.

When using supernovae to measure the cosmological magnitude-redshift relation, the redshift used should be entirely due to the expansion of the universe. In practice this is never the case, as large-scale structure in the universe induces peculiar motions so that the measured redshift contains some contribution from peculiar velocities.

Systematic peculiar velocity effects can arise in a number of ways. These include:

- Dipole effects, which occur due to our own peculiar motion. In the simplest case this can be accounted for using the dipole we observe in the cosmic microwave background (CMB). However, this needs to be modified when calculating our velocity relative to local galaxies that share some of our motion with respect to the CMB.
- Coherent flows, which cause correlated redshift offsets in distant sources that are close enough neighbours to share gravitational attraction to common large scale structure.
- Monopole effects that mimic expansion, which can arise if we are in a local over- or under-density. These also contribute dipole effects if we are off-centre from the density fluctuation.

All these peculiar velocities are manifestations of coherent flows in the universe. We consider the lowest order coherent flows (monopole and dipole) separately because they have the largest systematic effects. Moreover, it is relatively simple to correct for the dipole effect (Section 2) while higher-order coherent motions can currently only be taken into account statistically (Section 3). The monopole has a potentially large systematic effect that is difficult to correct for, so we consider how this can be mitigated (Section 4).

1.1. Background

When we compare the precision of redshift (z) measurements with the precision of apparent magnitude (m) measurements we are primarily concerned with their effect on the Hubble diagram (rather than the relative precision as measured by $\Delta z/z$ and $\Delta m/m$). The effect on the Hubble diagram can be quantified by considering the slope of the magnitude-redshift relation, dm/dz . Indeed, the standard method for including redshift uncertainties (σ_z) in cosmological analyses is to convert them to magnitude uncertainties (σ_m) using the dm/dz derived from a fiducial cosmological model (see Appendix A for an outline of the procedure). The conversion between a redshift uncertainty and a magnitude uncertainty is shown in Figure 1, for a few different redshifts. At higher redshifts the magnitude-redshift relation is flatter (dm/dz is smaller) which means large redshift uncertainties generate only small magnitude uncertainties. At low redshifts the converse is true, and small redshift uncertainties give large magnitude uncertainties.

The dominant source of intrinsic redshift dispersion (that is always included in cosmological analyses) is the effect of random peculiar velocities. These are usually taken to be about¹⁶ $\sigma_v^{\text{pec}} = 300\text{km s}^{-1}$, which according to $v^{\text{pec}} = cz^{\text{pec}}$ corresponds to an error in redshift of $\sigma_z^{\text{pec}} = 0.001$. This redshift uncertainty gives a non-negligible magnitude uncertainty of $\sigma_m^{\text{pec}} = 0.2$ for objects at redshift $z = 0.01$, which reduces to $\sigma_m^{\text{pec}} = 0.02$ for objects at $z = 0.1$. These values should be compared with the intrinsic diversity in supernova magnitudes of $\sigma_m^{\text{int}} \approx 0.1$ and the observational magnitude uncertainty (including the uncertainty in fitting the SN light curves) of $\sigma_m^{\text{meas}} \lesssim 0.1$ for the most distant supernovae included in most samples (closer ones have smaller observational uncertainty).

The observational uncertainty in redshift is typically $\sigma_z^{\text{spec}} \approx 0.0005$ for SN host-galaxy-based redshifts measured by SDSS, and $\sigma_z^{\text{spec}} \approx 0.005$ for redshifts based on the supernova spectra alone (Zheng et al. 2008). So the observational uncertainty is of similar magnitude to the intrinsic scatter due to peculiar motions. Some of these sources of uncertainty are depicted in Fig. 1 for comparison.

In this paper we use the Sloan Digital Sky Survey-II Supernova Survey (SDSS-II SN Survey York et al. 2000; Holtzman et al. 2008; Frieman et al. 2008; Sako et al.

¹⁶ For the SDSS sample Kessler et al. (2009) use $\sigma_v^{\text{pec}} = 300\text{km s}^{-1}$ for the random peculiar motions added in quadrature with $\sigma_v^{\text{pec}} = 200\text{km s}^{-1}$ for the internal velocities, giving a total $\sigma_v^{\text{pec}} = 360\text{km s}^{-1}$, corresponding to $\sigma_z^{\text{pec}} = 0.0012$. For the ESSENCE sample Wood-Vasey et al. (2007) uses $\sigma_v^{\text{pec}} = 400\text{km s}^{-1}$.

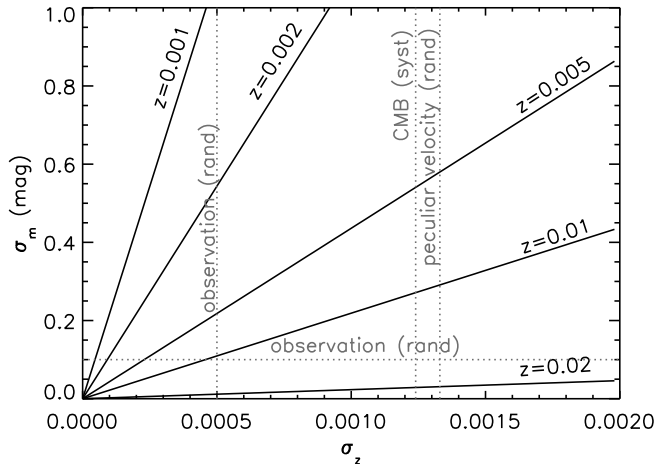


FIG. 1.— Plot of the conversion between a redshift uncertainty σ_z and a magnitude uncertainty σ_m , for a variety of redshifts between $z = 0.001$ and $z = 0.02$ as labelled. Dotted lines depict the typical redshift dispersion from random peculiar velocities, and the observational uncertainties in magnitude and redshift (the observational uncertainty for σ_z assumes we have redshifts from host galaxy spectra, when only SN spectra are available the redshift error is an order of magnitude higher). Those random contributions are all marked ‘(rand)’, while the other dotted line depicting ‘CMB (syst)’ shows the maximum systematic shift in redshift caused by the CMB dipole. This figure shows why the low-redshift cutoff of $z = 0.02$ is appropriate, because above this redshift all redshift uncertainties are significantly smaller than the observational magnitude uncertainty. The conversion has been done for the $(\Omega_m, \Omega_\Lambda) = (0.3, 0.7)$ model, but there is negligible difference between this and most plausible homogeneous cosmological models over this redshift range (including the empty model and a model without a cosmological constant).

2008) as a case study, in combination with nearby SNe at lower redshift. For the SDSS-II SN Survey repeat images were taken of an equatorial stripe, 2.5 degrees wide and about 120 degrees long centred on RA 23.5hr (SDSS Stripe 82). Over three years about 500 spectroscopically confirmed Type Ia supernovae were discovered in the redshift range $0.05 < z < 0.4$. The first year’s data including 103 supernovae were published in Holtzman et al. (2008) and analysed in Kessler et al. (2009, hereafter referred to as K09)¹⁷ who combined these with a re-analysis of existing data to make a coherent sample of 288 supernovae that were used to measure cosmological parameters. It is this data set that we use here, focussing on several of the subsets they define to demonstrate the effect of different redshift ranges.

Since the SDSS sample concentrates on relatively nearby supernovae ($0.05 \lesssim z \lesssim 0.4$) the peculiar velocity contribution is a more significant proportion of the total redshift than in surveys that focus on higher redshifts such as ESSENCE (Wood-Vasey et al. 2007), SuperNova Legacy Survey (Astier et al. 2006), and Higher- z (Riess et al. 2007). Moreover, the region of sky covered by the SDSS SN survey lies close to the direction of the CMB dipole (Fig. 2) so the alignment conspires to maximise the magnitude of the effect. For all these reasons the SDSS SN sample is an interesting one in which to test peculiar velocity effects.

In Section 2 we calculate the dipole corrections for the SDSS supernova sample, taking into account both the

CMB dipole correction and the contribution from our common local group motions. We then show the effect this correction has on the cosmological parameters derived (Sect. 2.3). Typically supernova surveys to date correct for the CMB, but not the local dipole. We demonstrate that this choice is justified.

In Section 3 we deal with the peculiar velocity of the supernova itself, which is typically treated as random scatter since the motions are expected to be largely random. This treatment is not entirely valid since galaxies (and the supernovae in them) preferentially fall into overdense regions, so objects in the same region of sky will tend to have correlated peculiar velocities. Detailed measurements of this effect may provide another technique for measuring the matter distribution of the universe (e.g. Neill et al. 2007; Hannestad et al. 2008). Here we assess the redshift dependence of correlated velocities and how to deal with them statistically (in the absence of measurements of the density field that would allow correction for correlations on an object-by-object basis).

Finally, we consider in Section. 4 the monopole that arises in an inhomogeneous universe because observers do not generally find themselves in a region of average density. Much attention has been given over the last few years to a possible Hubble Bubble — a proposed underdensity in our local universe that may explain some of the acceleration inferred from supernova data (Zehavi et al. 1998; Giovanelli et al. 1999; Hudson et al. 2004; Jha et al. 2006; Conley et al. 2007). Such an underdensity is very difficult to detect (if we are at the centre of it) because it imprints a systematic redshift on every source that is in large part degenerate with the cosmological redshift. To completely explain the observed acceleration the size of the underdensity would have to be far larger than one expects for a typical density fluctuation in a Λ CDM universe (Furlanetto & Piran 2006; Garcia-Bellido & Haugbølle 2008; Zibin et al. 2008; Alexander et al. 2009). However, since we are trying to test whether Λ CDM is the correct model for the universe, we enter a circular argument if we reject propositions on the basis that they are not expected within Λ CDM. In any case, a smaller underdensity such as *is* expected in Λ CDM can still significantly bias the cosmological results (Sinclair et al. 2010).

Supernova studies usually discard supernovae below a certain redshift that are particularly susceptible to this kind of monopole systematic.¹⁸ In Section 4 we analyse the likely monopole contribution for density fluctuations on a scale observed in galaxy redshift surveys (Geller et al. 1997; Croton et al. 2004; Hoyle & Vogeley 2004; Patiri et al. 2006). We model the effect of imposing a low redshift cutoff and find that the restriction of $z \geq 0.02$ imposed by the SDSS-II SN Survey based on empirical considerations (Kessler et al. 2009) is also theoretically justified. However, we also note that a local under- or over-density leaves an irreducible systematic error on our cosmological inferences, even when one imposes a low- z cut that excises all the data within the

¹⁸ The motivation is not primarily to avoid a monopole systematic but rather because at low-redshifts peculiar velocities are a significant proportion of the cosmological redshift and add excessive scatter to the Hubble diagram. Nevertheless, rejection of low-redshift objects also helps reduce the effect of any local Hubble-bubble, should one exist.

¹⁷ http://das.sdss.org/va/SNcosmology/sncosm09_fits.tar.gz

local density fluctuation.

1.2. Notation

We use the metric

$$ds^2 = -c^2 dt^2 + R(t)^2 [d\chi^2 + S_k^2(\chi) d\Theta^2], \quad (1)$$

where t is proper time, $R(t)$ is the scale factor with dimensions of length, χ is the dimensionless comoving coordinate, $S_k(\chi) = \sin(\chi), \chi, \sinh(\chi)$ for closed, flat, and open universes respectively, and $d\Theta$ encompasses the angular terms. The present day scale factor, $R_0 \equiv c/(H_0 \sqrt{|\Omega_k|})$, and the dimensionless scale factor is defined as $a = R/R_0$. Hubble's parameter is $H(z) = \dot{a}/a$, where an overdot represents differentiation with respect to proper time. The dimensionless comoving distance as a function of redshift is related to cosmological parameters by

$$\chi = \frac{c}{R_0} \int_0^z \frac{dz}{H(z)}. \quad (2)$$

Frequently we will need the comoving distance with units of length, for which we will use the shorthand $\tilde{\chi} \equiv R_0 \chi$.

2. DIPOLE CORRECTION

When using supernova redshifts to make cosmological inferences we need to remove the imprint of our own peculiar motion so that the redshift of the supernova is entirely due to the expansion of the universe. To first order this is straightforward, since we know our own velocity to high precision from measurements of the CMB dipole. Correcting for the CMB dipole is standard practise in all supernova cosmology analyses (e.g. Astier et al. 2006; Wood-Vasey et al. 2007; Riess et al. 2007; Kowalski et al. 2008; Kessler et al. 2009).

For nearby supernovae there is an additional subtlety that arises because they share some of our motion. The dipole correction should account for the relative velocity between the detector and the supernova, so applying the CMB dipole correction to nearby supernovae actually over-corrects the effect. Here we give the details of how the CMB correction is applied to SNe, noting some mathematical subtleties that are at times neglected, and assess the impact of neglecting the local dipole.

2.1. CMB dipole

We are moving at $\mathbf{v}_{\odot}^{\text{pec}} = 371 \text{ km s}^{-1}$ with respect to the CMB (Kogut et al. 1993; Bennett et al. 2003). This is small compared to the Hubble flow for all but the nearest objects, dropping to less than $\sim 1\%$ beyond a redshift of 0.1. Our motion thus contributes a maximum redshift change of $\sigma_z = 0.00124$ to sources that are directly aligned with the dipole. This is much less than the equivalent uncertainty in our magnitude measurement (see Fig. 1); it is only its coherence among SNe that can make it significant.

The direction of the CMB dipole in Galactic coordinates is toward $(\ell, b) = (263^\circ.85, 48^\circ.25)$ (Bennett et al. 2003); so the antipode direction lies at $(\ell, b) \approx (83^\circ.85, -48^\circ.25)$. The SDSS SN Stripe 82 consists of an equatorial strip between right ascension of approximately 20hr and 3hr (J2000), which corresponds to a field centre at Galactic coordinates $(\ell, b) \approx (84^\circ, -57^\circ)$. That means that the centre of the SDSS field is almost aligned with the negative direction of the CMB dipole.

2.1.1. Correcting for the dipole

The general relationship between redshift and *peculiar* velocity is,

$$1 + z^{\text{pec}} = \sqrt{\frac{1 + v^{\text{pec}}/c}{1 - v^{\text{pec}}/c}}, \quad (3)$$

which simplifies to $z^{\text{pec}} = v^{\text{pec}}/c$ in the non-relativistic limit.¹⁹ The redshift correction required to account for our velocity with respect to the CMB, \mathbf{v}_{\odot} , is

$$z_{\odot}^{\text{pec}} = -v_{\odot}^{\text{pec}}/c = \mathbf{v}_{\odot}^{\text{pec}} \cdot (-\mathbf{n})/c \quad (4)$$

where \mathbf{n} is the unit vector from the sun to the supernova. (The negative sign ensures that if we are moving in the direction of the supernova the resulting correction is a blueshift.)

The observed heliocentric redshift, z , is then related to the cosmological redshift, \bar{z} , by,²⁰

$$(1 + z) = (1 + \bar{z})(1 + z_{\odot}^{\text{pec}}). \quad (5)$$

Note that the NED velocity calculator (NASA/IPAC Extragalactic Database 2008) uses the approximation,

$$z \approx \bar{z} + z_{\odot}^{\text{pec}}. \quad (6)$$

This gives a fractional error²¹ of precisely z_{\odot}^{pec} , which is negligible for most circumstances.

The dipole not only shifts the redshift but also changes the apparent magnitude of the source due to the Doppler shift of the photon energy and relativistic beaming. The CMB dipole therefore also has an effect on the *luminosity distance* calculated from the magnitude of a supernova (Sasaki 1987; Pyne & Birkinshaw 1996; Bonvin et al. 2006a; Cooray & Caldwell 2006; Hui & Greene 2006). This arises because the luminosity distance is related to the comoving distance, χ , by (recalling that overbars refer to observations made from the CMB rest frame),

$$\bar{d}_L(\bar{z}) = (1 + \bar{z})R_0 S_k(\chi). \quad (7)$$

However, what we actually observe is (recalling that z is the observed redshift and considering for the moment only our own motion),

$$d_L(z) = (1 + z)R_0 S_k(\chi), \quad (8)$$

$$= (1 + \bar{z})(1 + z_{\odot}^{\text{pec}})R_0 S_k(\chi), \quad (9)$$

$$= \bar{d}_L(\bar{z})(1 + z_{\odot}^{\text{pec}}). \quad (10)$$

So both the redshift and the luminosity distance need to be corrected for the effect of the dipole.²²

¹⁹ Note that the special relativistic velocity-redshift relation is *not* appropriate for recession velocities (the velocity that appears in Hubble's Law), for which special relativistic corrections should *never* be applied (Davis & Lineweaver 2004, 2005).

²⁰ This assumes the observer has already corrected both for the motion of the Earth around the Sun, which contributes up to 30 km s^{-1} depending on the time of observation and for atmospheric refraction, which contributes up to 90 km s^{-1} (the index of refraction of air is 1.0003, so $\Delta z = 0.0003$ and $c\Delta z = 90 \text{ km s}^{-1}$). Usually this is done as a standard step in wavelength calibration.

²¹ Rearranging Eq. 5 and Eq. 6 gives $\frac{\bar{z}^{\text{NED}} - \bar{z}}{\bar{z}} = z_{\odot}^{\text{pec}}$.

²² You may be concerned that in going from Eq. 8 to Eq. 9 we've neglected the factor of z in the calculation of $\chi = (c/R_0) \int_0^z d\bar{z}/H(\bar{z})$. However, this cosmological redshifting is in-

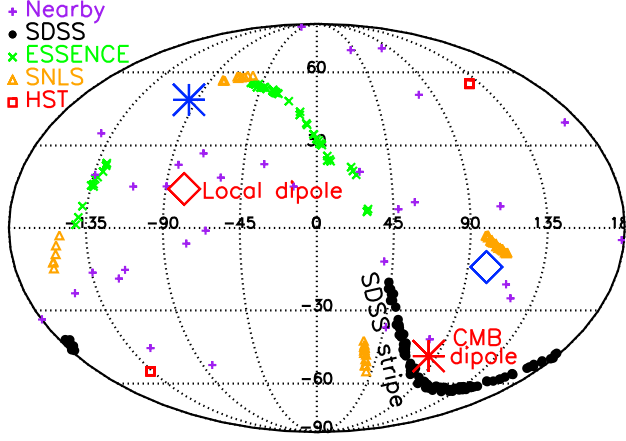


FIG. 2.— Map of the distribution of supernovae in the Nearby, SDSS, ESSENCE, SNLS, and HST samples in Galactic coordinates with the local ($z \sim 0.1$) dipole indicated by diamonds and the CMB dipole indicated by stars. The centre of the SDSS-II SN stripe lies close to the direction of the CMB dipole, which makes it important to carefully correct the SDSS sample for the effects of the dipole. The local dipole is measured with respect to the CMB and is in approximately the opposite direction since galaxies in our local neighbourhood tend to share some of our peculiar velocity with respect to the CMB. See the electronic edition of the Journal for a color version of this figure.

Alternatively, one can choose to correct for both in one fell swoop by correcting the observed luminosity distance at redshift z to the luminosity distance that would have been observed at redshift z in the absence of peculiar velocities. This is the approach taken by the commonly used program `simple_cosfitter`.²³ Hui & Greene (2006) give the formula for $\bar{d}_L(z)$, which can be used to correct only the d_L values without correcting z . Considering only our own motion, Eq. 15 of Hui & Greene (2006) can be rearranged to give,

$$d_L(z) = \bar{d}_L(z) \left[1 + \frac{a_e}{a'_e R_0 T_k(\chi)} \mathbf{v}_0 \cdot \mathbf{n} \right], \quad (11)$$

where $a'_e \equiv da_e/d\tau$ represents the derivative of the scale factor with respect to conformal time, evaluated at the time of emission,²⁴ and here we have kept the curvature dependence explicit, with $T_k(\chi) \equiv \tan(\chi), \chi$, and $\tanh(\chi)$ in closed, flat, and open universes respectively.

2.1.2. Correcting for the dipole and the source's motion

When there are two peculiar velocities to correct, such as when accounting for the supernova's motion²⁵ with

dependent of the motion of the emitter or observer, and therefore does not need correcting for peculiar velocities. As long as we correct the redshift of the supernova to the CMB frame our theoretical model comparison will be correct.

²³ http://qold.astro.utoronto.ca/conley/simple_cosfitter/html/

²⁴ We give conformal time dimensions of time, so $d\tau = dt/a$ and the conformal time derivative is related to the proper time derivative (denoted by an overdot) according to

$$a' = \frac{da}{dt} \frac{dt}{d\tau} = \dot{a}a. \quad (12)$$

²⁵ The additional redshift due to the supernova's motion is

$$z_{\text{SN}}^{\text{pec}} = v_{\text{SN}}^{\text{pec}}/c = \mathbf{v}_{\text{SN}}^{\text{pec}} \cdot \mathbf{n}/c, \quad (13)$$

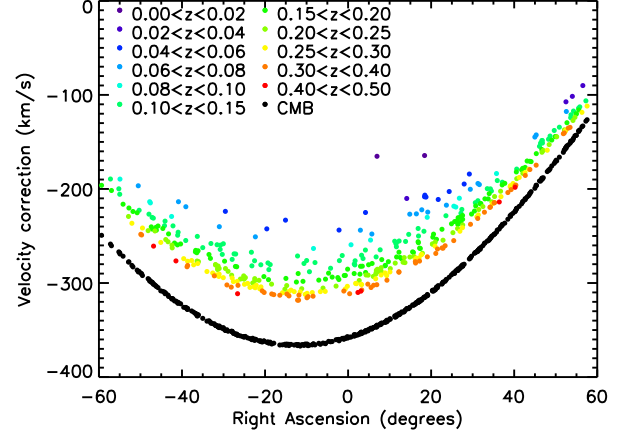


FIG. 3.— Peculiar velocity correction required for the SDSS sample, plotted as a function of right ascension (J2000). The SDSS SN sample spans an equatorial strip, and thus the peculiar velocity correction is systematic with right ascension. The CMB dipole correction is shown in black, while the local dipole correction, which is more relevant for low-redshift sources, is shown as shaded points, with different shades representing different redshift ranges. See the electronic edition of the Journal for a color version of this figure.

respect to the CMB ($z_{\text{SN}}^{\text{pec}}$) in addition to our own motion, one uses

$$(1+z) = (1+\bar{z})(1+z_{\odot}^{\text{pec}})(1+z_{\text{SN}}^{\text{pec}}). \quad (14)$$

This equation is valid even for relativistic velocities, but in the literature it is more common to encounter approximate formulae such as (Hui & Greene 2006),

$$(1+z) = (1+\bar{z})(1 - \mathbf{v}_{\odot} \cdot \mathbf{n}/c + \mathbf{v}_{\text{SN}} \cdot \mathbf{n}/c), \quad (15)$$

$$= (1+\bar{z})(1 + z_{\odot}^{\text{pec}} + z_{\text{SN}}^{\text{pec}}), \quad (16)$$

which are perfectly appropriate for the low velocities we encounter in almost all practical situations.

When including the source motion the correction to the luminosity distance becomes,

$$d_L(z) = \bar{d}_L(\bar{z})(1+z_{\odot}^{\text{pec}})(1+z_{\text{SN}}^{\text{pec}})^2. \quad (17)$$

Note that two factors of $(1+z_{\text{SN}}^{\text{pec}})$ enter the luminosity distance correction. One is due to the Doppler shifting of the photons, the other is due to relativistic beaming.

2.2. Local dipole

Galaxies in our local universe share some of our locally induced peculiar motion, so our velocity relative to our neighbours is lower than our velocity with respect to the CMB. For example, below redshifts of ~ 0.02 we are strongly influenced by the Great Attractor and the Perseus-Pisces Supercluster (Erdoğdu et al. 2006). Thus the lowest redshift supernovae in the SDSS sample should be corrected for this more local dipole rather than the CMB dipole.

Bonvin et al. (2006b) measured our dipole relative to the nearby sample of 44 supernovae used by (Astier et al. 2006) and found it to be consistent with the CMB dipole, although with large uncertainties (about $\pm 30^\circ$

where again \mathbf{n} is the unit vector from the sun to the supernova and $\mathbf{v}_{\text{SN}}^{\text{pec}}$ is measured with respect to the CMB.

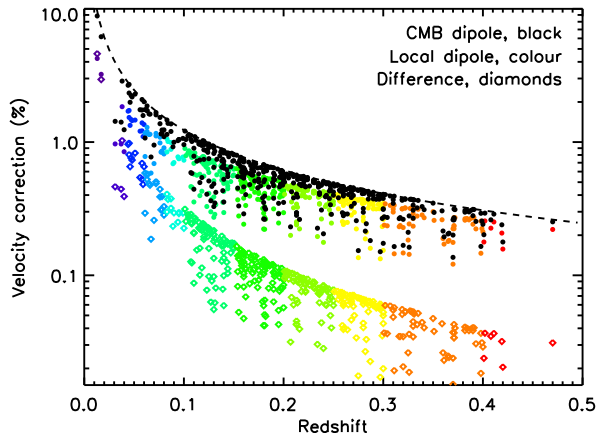


FIG. 4.— Similar to Figure 3, but with the correction expressed as a percentage and plotted against redshift. The peculiar velocity correction taking into account the local dipole (shaded filled circles) is compared to the CMB dipole correction (black filled circles). The difference between the two is shown as shaded diamonds. The dashed line shows the theoretical maximum correction that would be applied to an object directly aligned with the CMB dipole: a constant peculiar velocity correction of 371km s^{-1} that decreases with redshift only because it is a decreasing fraction of the total redshift. The difference between the CMB and local dipole correction is only significant for the closest supernovae in the sample, with a $\sim 4\%$ correction in redshift when $z < 0.02$ but a correction of less than 1% for supernovae with $z \gtrsim 0.05$. See the electronic edition of the Journal for a color version of this figure.

directional uncertainty, and 200km s^{-1} magnitude uncertainty). Haugbølle et al. (2007) were able to more precisely measure the velocity flow of the local universe using the 133 low-redshift type Ia supernovae from Jha et al. (2007). At a redshift of ~ 0.02 ($60h^{-1}\text{Mpc}$) they find a dipole amplitude of $239^{+70}_{-96}\text{ km s}^{-1}$ in the direction $\ell \approx 281^\circ \pm 23^\circ$, $b \approx 14^\circ \pm 16^\circ$ (measured relative to the CMB rest frame). In Figure 2 this dipole is marked by diamonds. The magnitude of this dipole decreases with redshift.

This result is consistent with a recent compilation by Watkins et al. (2009) who combined nine peculiar velocity datasets measured using five different methods of distance estimation (surface brightness fluctuations; fundamental plane; type Ia supernovae; Tully-Fisher; and brightest cluster galaxies) and concluded that the bulk flow within a Gaussian window of radius $50h^{-1}\text{Mpc}$ is $407 \pm 81\text{km s}^{-1}$ toward $\ell = 287^\circ \pm 9^\circ$, $b = 8^\circ \pm 6^\circ$. They note that the magnitude of this flow is larger than would be predicted by standard cosmological models based on the best cosmological parameter estimates from WMAP (Komatsu et al. 2009). An even more significant deviation from the predictions of ΛCDM was found by Kashlinsky et al. (2008, 2009), who measured the kinematic Sunyaev-Zel’dovich effect of the CMB in the direction of known galaxy clusters. Their observations were at higher redshift ($z \sim 0.1$ or about $300h^{-1}\text{Mpc}$) and they found a considerably higher amplitude bulk flow ($600\text{--}1000\text{km s}^{-1}$) than measured by Watkins et al. (2009) and Haugbølle et al. (2007), but the dipole direction was the same. As well as differing from the theoretical prediction, this result does contradict the measurement by Haugbølle et al. (2007) of a dipole amplitude

that decreases with distance.

Given the uncertainty in the redshift dependence of the local dipole it is premature to apply any correction before publishing observational data. Nevertheless we want to estimate the effect the local dipole has on cosmological inferences. Since the low-redshift supernova data is the most influenced by redshift uncertainties, it is sufficient to use the consistent estimates of Haugbølle et al. (2007) and Watkins et al. (2009) at around $z \sim 0.015$ for the local dipole magnitude. We then choose to use the redshift dependence measured by Haugbølle et al. (2007), in which the dipole magnitude decreases with distance. This relation is qualitatively what is predicted by standard ΛCDM models; however, quantitatively it does not drop as quickly as one expects from simulations. Our choice of redshift dependence therefore lies between the theoretical predictions and the kinematic SZ results. The precise choice is not significant because it is the low-redshift points that have the largest dm/dz effect.

2.3. Dipole results

The magnitude of the correction due to the local dipole is shown for the SDSS supernovae as a function of right ascension in Figure 3. The black points show the correction for the CMB dipole, ignoring the local dipole. The shaded points show the correction after the contribution from the local-dipole has been included. The velocity correction required is less than the CMB correction because within the local group we are all moving towards the same large scale structures and thus our relative velocity is smaller than our velocity with respect to the CMB. The different shades in the figure represent different redshift ranges, with the lowest redshifts receiving the largest local-dipole correction, and the higher-redshifts tending towards the CMB correction.

Figure 4 shows the same information plotted as a function of redshift and expressed as a percentage ($\Delta z/z \times 100\%$). Here the dashed line shows the theoretical maximum correction required due to the CMB dipole – as occurs for objects directly aligned with the dipole. The size of this Δz correction is constant but its fractional contribution decreases with redshift. The black points show the CMB correction for the SDSS supernovae taking into account their position on the sky. The shaded circles under the black CMB points show the correction for the local dipole. The shaded diamonds show the difference between the CMB and local dipoles (the amount by which applying the CMB dipole overcorrects). This difference does decrease in absolute terms as a function of redshift, resulting in the sharper decline with redshift than the CMB correction. The CMB dipole correction drops to less than about 1% beyond redshifts of $z \gtrsim 0.13$. The difference between that and the local dipole correction becomes negligible much faster, reducing to less than 1% beyond redshifts of $z \gtrsim 0.05$.

All the major supernova datasets, such as the recent ones compiled by ESSENCE (Miknaitis et al. 2007; Wood-Vasey et al. 2007), SuperNova Legacy Survey (Astier et al. 2006), HST (Riess et al. 2007), Supernova Cosmology Project (Kowalski et al. 2008, Union), Centre for Astrophysics (Hicken et al. 2009, Constitution), and SDSS (Kessler et al. 2009) have the CMB dipole correction applied, but none correct for the local dipole.

In Figure 5 we show the shift in cosmological param-

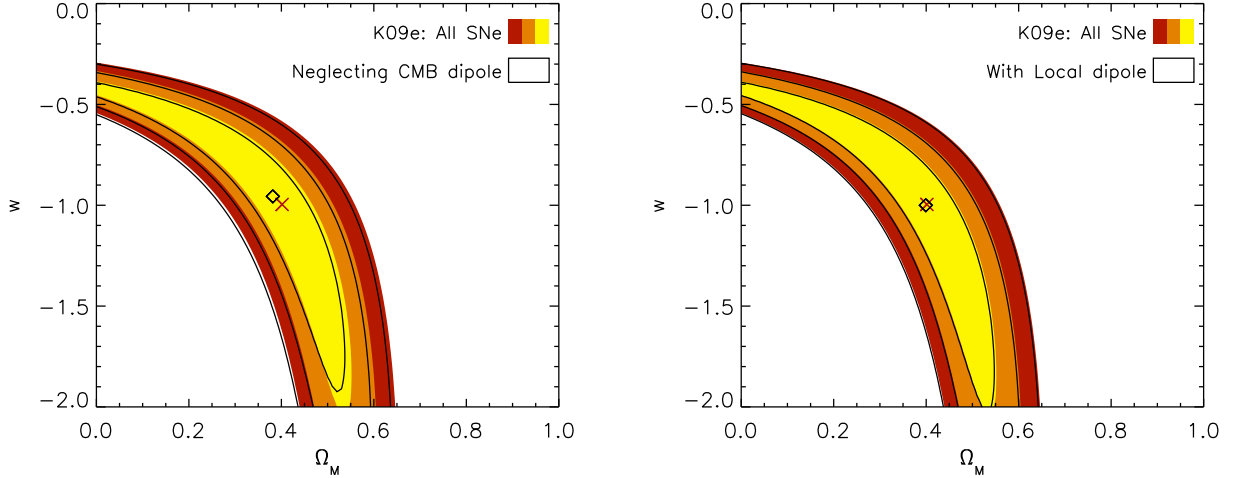


FIG. 5.— Cosmological parameter likelihood surfaces in the flat w CDM model (one, two, and three sigma). The shaded contours display the K09 data set e (full sample) and the same contours are displayed in both the top and bottom panels for reference. The red cross indicates the point of maximum likelihood for the K09 data. In addition, the top panel shows an alternative analysis of the same data in which the CMB dipole correction is not applied (black curves). The bottom panel shows an alternative analysis where the both the CMB dipole and local dipole corrections are applied to the SN data. The point of maximum likelihood for each of these alternative analyses is indicated by the black diamond on the top and bottom panels respectively. Only shifts perpendicular to the long axis of the contours are significant, because shifts along the long axis represent very small changes in χ^2 and are well constrained by other measurements (e.g. CMB and BAO). Correcting for the CMB dipole shifts the contours by about 15% of 1σ , while the shift due to the local dipole is negligible. See the electronic edition of the Journal for a color version of this figure.

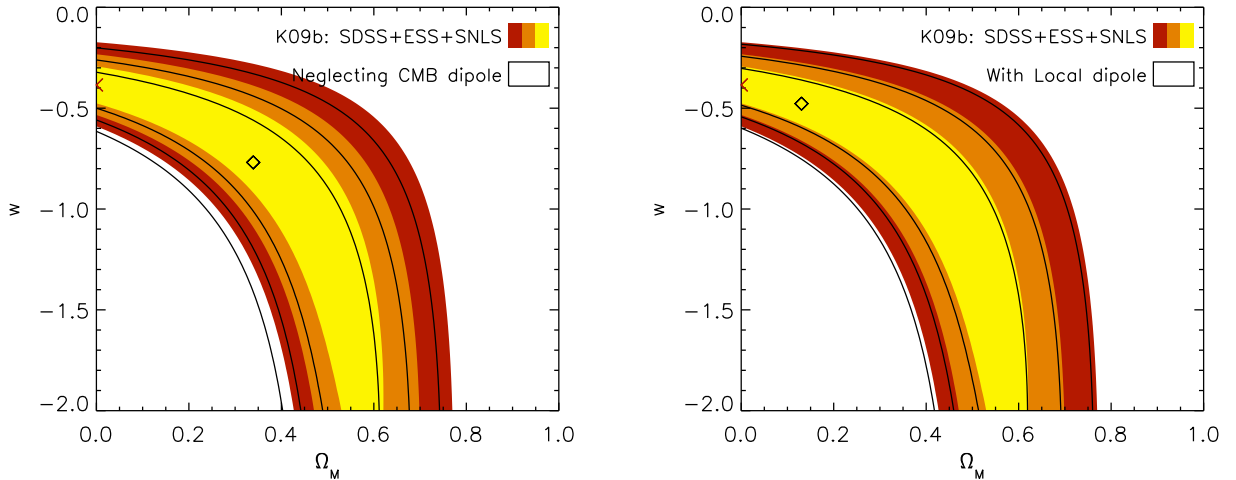


FIG. 6.— Similar to Fig. 5, but using dataset ‘b’ from K09, which includes the SDSS, ESSENCE, and SNLS data. This dataset is more sensitive to dipole corrections because it excludes the relatively isotropically distributed nearby sample and relies on the SDSS sample as the local anchor of the Hubble diagram. The best fit values are shown (as red crosses for K09, black diamonds for the two variations), but these are not particularly good indicators because the best fit in this case is on the edge of the parameter space explored. More indicative of the magnitude of the effect is the amount that the contours shift. The CMB dipole shifts the contours by about 0.2σ , corresponding to a $\Delta w \sim 0.04$ along the line of constant $\Omega_M = 0.3$, while the shift due to the local dipole is small ($\Delta w \lesssim 0.01$). See the electronic edition of the Journal for a color version of this figure.

ter estimates that occurs when we ignore the CMB dipole correction (upper) and when we add the additional correction due to the local dipole (lower).

To make this comparison we have used the MLCS2k2 version of data set ‘e’ from K09, which includes the new supernovae from the SDSS collaboration combined with the high-redshift ESSENCE, SNLS, and HST data along with the low-redshift sample (Hamuy et al. 1996; Riess et al. 1999; Jha et al. 2006).

The choice of dataset is important, so we also show in Figure 6 the effect of the dipole on data set ‘b’ from K09, which *excludes* the relatively isotropically distributed

nearby sample and relies on the SDSS sample as the nearby anchor for the Hubble diagram. This makes it more sensitive to the dipole correction.

It is clear from these figures that the CMB dipole correction is important. Neglecting it introduces a systematic shift of $\Delta w = 0.04$ when considering the best fit w at a constant $\Omega_M \sim 0.3$. This represents about 20% of one standard deviation at the current accuracy levels, but will become ever more important as groups strive to decrease the uncertainty on w below 5%. This CMB correction is already routinely applied to supernova data sets and it can be done to very high precision thanks to

the accurate measurements of the CMB dipole. However, the characteristics of the local dipole are much more uncertain. Given the assumptions we have outlined here, Figure 5 shows the contribution from the local dipole is currently negligible, giving a shift of $\Delta w \lesssim 0.01$. For the current sample, therefore, K09 are justified in correcting solely for the CMB dipole and ignoring local non-CMB contributions. This may not be true in the future when more data are available, particularly data at redshifts below 0.05.

The lower sensitivity to dipole corrections shown in Figure 5 compared to Figure 6 demonstrates that choosing an isotropically distributed local supernova sample protects us, to a great extent, from systematic errors due to any unaccounted-for local dipole. In the next section we will see that isotropic samples do not save us from the effects of higher-order motions.

3. COHERENT FLOWS

The next peculiar velocity effect we consider is the impact of coherent bulk motions. Large scale structure introduces correlated peculiar velocities as neighbouring galaxies, and the supernovae they host, fall towards the same overdensities. Ignoring these correlations underestimates the uncertainty in our cosmological inferences. The effect is particularly important at low redshift where supernovae will tend to be physically closer to each other (as a function of angular separation on the sky).

These coherent flows are the higher-order manifestations of the gravitational influence of large scale structure, beyond the local dipole we discussed in Sect. 2. This exercise is analogous to subtracting the dipole from the CMB and considering the residual fluctuations.

The reason correlated velocities have a deleterious impact on standard supernova cosmology arises because two correlated supernovae can not be statistically averaged in such a way so as to reduce the error in proportion to the square-root of the number of supernovae, as is usually assumed. Correlations mean the data are not randomly distributed about the central value, so the uncertainties do not average out exactly and there remains a residual error even in the limit of an infinite number of data points.

Put simply, two correlated supernovae could both lie above (or below) the magnitude-redshift relation of the correct underlying model, so taking the average of the two will not reduce to the correct model. The amount of correlation determines how much residual uncertainty is required to take this into account.

Here we assess the impact of coherent flows on the error estimates and thus the cosmological constraints derived from supernovae. We first calculate the expected statistical correlations in the peculiar velocities of galaxies as a function of their distance from each other based on a Λ CDM model. We convert this into an observationally useful measure by converting it to the expected covariance in magnitudes as a function of angular separation and redshift separation. We then apply the results to the low-redshift supernovae in our sample and calculate the difference in the uncertainty estimates on the cosmological parameters.

In the next section we summarize how to calculate correlations and include this information in the likelihood calculation for cosmological models. We then demon-

strate the effect on the error estimates and the best-fit values of the cosmological parameters.

3.1. Calculating correlations

Recall that supernova cosmology aims to fit the observations of apparent magnitude, m , and redshift, z of a supernova to the following relation,

$$m(z) = 5 \log_{10} d_L(z) + \mathcal{M}, \quad (18)$$

where d_L is the luminosity distance (in units of 10pc) and \mathcal{M} is a constant incorporating the absolute magnitude of the supernova and Hubble's constant. The luminosity distance is a function of the cosmological parameters we want to fit.

The likelihood of a particular model, in a gaussian distribution, is proportional to $e^{-\chi^2/2}$. Let \hat{m}_i represent the i th measurement and m_i the corresponding model prediction. When all data points are independent, χ^2 is given by,²⁶

$$\chi^2 = \sum_i \frac{(\hat{m}_i - m_i)^2}{\sigma_i^2}. \quad (19)$$

Here $\sigma_i \equiv \sigma_{m_i}$ is the magnitude uncertainty on m_i . However, when data points are correlated the more general form of χ^2 is given by,

$$\chi^2 = \sum_{i,j} (\hat{m}_i - m_i) C_{ij}^{-1} (\hat{m}_j - m_j), \quad (20)$$

where the covariance matrix,

$$C_{ij} \equiv \langle \delta \hat{m}_i \delta \hat{m}_j \rangle, \quad (21)$$

quantifies how likely two supernovae are to have the same offset from the correct model. The factor $\delta \hat{m}_i \equiv \hat{m}_i - \langle \hat{m}_i \rangle$ designates how far the i th data point deviates from the mean of the observational data.

The covariance matrix can be divided into the random component σ_i and the correlated component, which we consider to be only due to peculiar velocities, C_{ij}^{vel} ,

$$C_{ij} = \sigma_i \delta_{ij} + C_{ij}^{\text{vel}}. \quad (22)$$

As discussed in Hui & Greene (2006), there are a wider variety of large scale structure induced fluctuations than are accounted for in Eq. 22. For instance, lensing introduces correlated noise in addition to Poissonian fluctuations. There are also fluctuations due to gravitational redshift and the integrated Sachs-Wolfe effect. It can be shown that all these effects can be neglected for surveys of current practical interest (Hui & Greene 2006).

The random uncertainties, which contribute to the diagonal part of C_{ij} , include the intrinsic diversity in the supernova population, σ_i^{intr} , the scatter due to measurement uncertainty, σ_i^{meas} , and the contribution from random peculiar velocities, σ_i^{vel} . Although random peculiar velocities primarily add dispersion in the apparent redshift of the sources (the effect on the luminosity is smaller and is usually neglected), this is usually converted to a dispersion in magnitude and added in quadrature to the

²⁶ In this paragraph χ^2 represents the statistic, not the comoving coordinate squared.

other magnitude uncertainties (see Appendix A for more detail),

$$\sigma_i^2 = \sigma_i^{\text{intr}2} + \sigma_i^{\text{meas}2} + \sigma_i^{\text{vel}2}. \quad (23)$$

Since random peculiar velocities are taken into account by this diagonal term we set all diagonal terms $C_{ij}^{\text{vel}} = 0$. Alternatively we could remove σ_i^{vel} and reinstate them as the diagonal elements of C_{ij}^{vel} .

The velocity correlation function is defined to be,

$$\xi_{ij}^{\text{vel}} \equiv \langle (\mathbf{v}_i \cdot \hat{\mathbf{x}}_i)(\mathbf{v}_j \cdot \hat{\mathbf{x}}_j) \rangle \quad (24)$$

where $\hat{\mathbf{x}}_i$ and $\hat{\mathbf{x}}_j$ represent the unit vectors pointing towards SNe i and j respectively, and \mathbf{v}_i and \mathbf{v}_j represent the velocity vectors of each supernova's motion.

The peculiar-motion-induced magnitude covariance is related to the velocity correlation function ξ_{ij}^{vel} by,

$$C_{ij}^{\text{vel}} = \left[\frac{5}{c \ln 10} \right]^2 \left[1 - \frac{a_i}{a'_i} \frac{c}{\tilde{\chi}_i} \right] \left[1 - \frac{a_j}{a'_j} \frac{c}{\tilde{\chi}_j} \right] \xi_{ij}^{\text{vel}}, \quad (25)$$

where c is the speed of light, $\tilde{\chi} \equiv R_0 \chi$ is the radial comoving distance, $a = R/R_0$ is the normalised scale factor, and the prime denotes the conformal time derivative. All quantities with a subscript i or j are to be evaluated at the redshift of the SN in question. For a non-flat universe $\tilde{\chi} \rightarrow R_0 T_k(\chi)$.

A numerical code to compute both ξ_{ij}^{vel} and C_{ij}^{vel} for a pair of points at arbitrary redshifts and angular separation in the standard cosmological model of Λ CDM is available at <http://www.astro.columbia.edu/~lhui/PairV>. We illustrate the results of that code in Figs. 7 and 8, and in what follows we explain the theory behind those calculations.

To calculate the expected velocity correlation function given a theoretical model we need information about how structure grows. To first order this is given by the linear growth factor $D(z) \equiv \delta(z)/\delta(0)$, where the overdensity $\delta = (\rho - \langle \rho \rangle)/\langle \rho \rangle$. As input we also use the mass power spectrum of density fluctuations observed at the present time $P(k)_{z=0}$, where k is the comoving wavenumber (inverse distance).

Using these we can estimate the distribution of peculiar velocities expected in a particular theoretical model. Concentrating for the moment only on the dispersion (the diagonal terms in the velocity correlation function), one finds the dispersion in peculiar velocities to be (Hui & Greene 2006),

$$\sigma_{v_i}^{\text{vel}2} \equiv \xi_{ii}^{\text{vel}} = D'(z_i)^2 \int_0^\infty \frac{dk}{6\pi^2} P(k)_{z=0}, \quad (26)$$

which results in a dispersion in apparent magnitude of,

$$\sigma_i^{\text{vel}2} = \left[\frac{5}{c \ln 10} \right]^2 \left[1 - \frac{a_i}{a'_i} \frac{c}{\tilde{\chi}_i} \right]^2 \sigma_{v_i}^{\text{vel}2}. \quad (27)$$

In principle this dispersion is sensitive to non-linear fluctuations, but the velocity power spectrum weights larger-scale modes more than the density power spectrum does and we find that when using the linear mass power spectrum for a Λ CDM model the resulting value for σ_{v_i} agrees

with the canonical value of 300 km/s to better than 10% for all redshifts of interest. The off-diagonal components of C_{ij} should be at least as well fit by linear theory since they are less sensitive to small-scale structure than σ_{v_i} .

The off-diagonal part of C_{ij} , given by C_{ij}^{vel} in Eq. 22, accounts for the effects of correlated peculiar flows. Expressing this quantity in an observer-centric form Hui & Greene (2006) show that for a flat universe,

$$C_{ij}^{\text{vel}} = \left[\frac{5}{c \ln 10} \right]^2 \left[1 - \frac{a_i}{a'_i} \frac{c}{\tilde{\chi}_i} \right] \left[1 - \frac{a_j}{a'_j} \frac{c}{\tilde{\chi}_j} \right] \times \quad (28)$$

$$D'_i D'_j \int_0^\infty \frac{dk}{2\pi^2} P(k)_{z=0} \times$$

$$\sum_{\ell=0}^\infty (2\ell+1) j'_\ell(k\tilde{\chi}_i) j'_\ell(k\tilde{\chi}_j) \mathcal{P}_\ell(\hat{\mathbf{x}}_i \cdot \hat{\mathbf{x}}_j),$$

where \mathcal{P}_ℓ is the Legendre polynomial, j_ℓ is the spherical Bessel function, and j'_ℓ is its derivative with respect to its argument. It is useful to note that $j'_\ell(x) = j_{\ell-1} - (\ell+1)j_\ell/x$. This observer-centric form can be derived from Eq. 22, D7, and D10 of Hui & Greene (2006), by setting the survey geometry to be two delta functions localized at the two SNe of interest.

An alternative separation-centric form for the same quantity is (Gorski 1988; Gordon et al. 2007),

$$C_{ij}^{\text{vel}} = \left[\frac{5}{c \ln 10} \right]^2 \left[1 - \frac{a_i}{a'_i} \frac{c}{\tilde{\chi}_i} \right] \left[1 - \frac{a_j}{a'_j} \frac{c}{\tilde{\chi}_j} \right] \times \quad (29)$$

$$[(\hat{\mathbf{x}}_i \cdot \hat{\mathbf{r}})(\hat{\mathbf{x}}_j \cdot \hat{\mathbf{r}})\Pi(r) + [\hat{\mathbf{x}}_i \cdot \hat{\mathbf{x}}_j - (\hat{\mathbf{x}}_i \cdot \hat{\mathbf{r}})(\hat{\mathbf{x}}_j \cdot \hat{\mathbf{r}})]\Sigma(r)]$$

$$\Pi(r) \equiv D'_i D'_j \int_0^\infty \frac{dk}{2\pi^2} P(k)_{z=0} \left[j_0(kr) - \frac{2j_1(kr)}{kr} \right]$$

$$\Sigma(r) \equiv D'_i D'_j \int_0^\infty \frac{dk}{2\pi^2} P(k)_{z=0} \frac{j_1(kr)}{kr}$$

where the comoving separation between the two SNe is given by r and $\hat{\mathbf{r}}$ is the unit vector pointing along the separation.

That Eq. (28) and (29) are equivalent is shown in Appendix B. The separation-centric form is useful for fast computation, while the observer-centric form is more directly linked to the observed velocity angular power spectrum. Note that these two equations are only strictly valid for a flat universe, since the derivation in Appendix B uses a plane-wave expansion that needs modification if the universe is not flat.

We are interested in the implications of deviating from the common practise of assuming all velocities are uncorrelated. In the next section we therefore test the impact of including C_{ij}^{vel} in the covariance matrix of the uncertainties for the supernova sample used by K09.

3.2. Correlation's impact on cosmology

We use a model linear power spectrum and growth function based on a fiducial flat- Λ CDM cosmology with $[h, \Omega_m, \Omega_b, \sigma_8, n] = [0.701, 0.2792, 0.046, 0.817, 0.96]$ to estimate C_{ij} as per Eq. 28. This allows us to calculate the likelihood that two supernovae will have correlated velocities based on their physical separation. We plot the amount of velocity correlation as a function of redshift

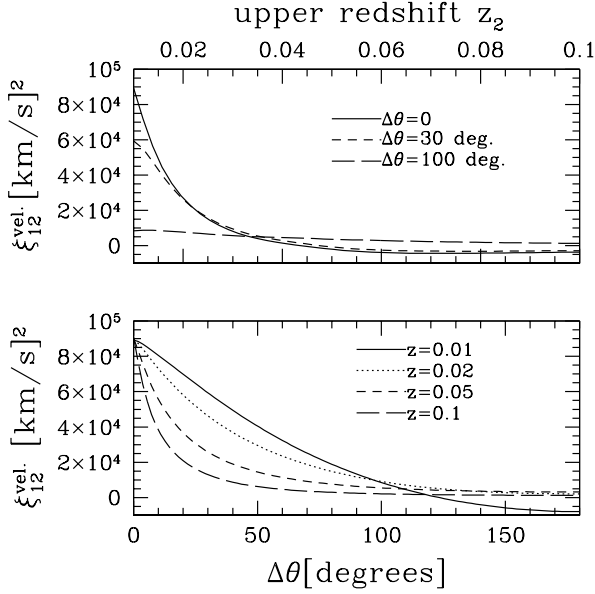


FIG. 7.— The velocity two-point correlation, ξ_{12} , in units of $(\text{km s}^{-1})^2$. The upper panel shows the correlation as a function of z_2 (the redshift of the higher redshift supernova) compared to a low-redshift supernova at a fixed $z_1 = 0.01$, for three different angular separations (0, 30 and 100 degrees). As the redshift separation increases the correlation diminishes. The lower panel shows the correlation as a function of angular separation, in the case where the two supernovae are at the same redshift ($z_2 = z_1 = 0.01, 0.02, 0.05$, and 0.1). For a fixed angular separation the correlation is most dramatic at low redshifts because this corresponds to a smaller physical distance than the same angular separation at high redshifts. ξ_{12} is given by the last two lines of Eq. 28.

and angular separations in Fig. 7, with the corresponding magnitude covariances shown in Fig. 8.

After applying that correction to the K09 sample we re-fit our cosmological models. We fit a flat w CDM model, allowing the matter density Ω_m and dark energy equation of state w to vary. (Note that we do not redo the velocity covariance approximation for each different model, but the differences would be small.) In addition to the supernova data we also include the same priors as K09, described in detail in their Section 8. Specifically, for Baryon Acoustic Oscillations (BAO) we use the (Eisenstein et al. 2005) result that the derived distance parameter, $A(z = 0.35) = 0.469 \pm 0.017$, and from the CMB we use the (Komatsu et al. 2009) result that the shift parameter $R(z = 1100) = 1.710 \pm 0.019$.

The low-redshift cutoff is usually applied in order to remove the effect of low-redshift peculiar velocities. Implementing a correlated velocity correction increases the error bars on all the low- z supernovae relative to the high- z supernovae. This effectively down-weights the lower redshift end of the Hubble diagram and thus has a similar effect to the low-redshift cutoff.

We first consider only the low-redshift supernovae, for which this gives the largest effect, i.e. the Low- z +SDSS sample ‘c’ from K09. As done in K09, we apply a low- z cut of $z_{\text{cut}} = 0.02$. In this case w increases by 0.02 when the distance correlations are included. Using the larger sample ‘d’ from K09 that also includes the higher redshift ESSENCE and SDSS data, we find w in-

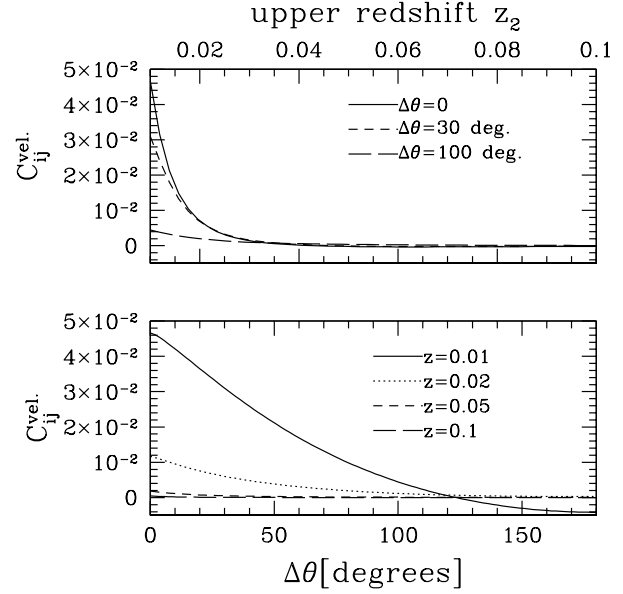


FIG. 8.— The magnitude covariance due to peculiar motion (Eq. 28). As for Fig. 7 the upper panel shows, for three different angular separations, the covariance between a $z_1 = 0.01$ source and a source at a higher redshift, z_2 . The lower panel shows for fixed redshifts ($z_2 = z_1 = 0.01, 0.02, 0.05$, and 0.1) how the covariance drops as the angular separation increases. To get a feel for how much additional uncertainty the correlated component adds to the uncorrelated dispersion consider that for these four redshifts the canonical 300 km s^{-1} dispersion corresponds to $\sigma_m^2 \sim (25, 10, 7, 5) \times 10^{-3}$ respectively (see Appendix A). So the strongest correlated uncertainties are an order of magnitude lower than the random dispersion. However, the random dispersion can be beaten down by raising the number of SNe, while the correlated covariance cannot. Thus, as the total number of SNe increases the correlated noise becomes comparatively more and more important.

creases by 0.014 due to the correlated velocities. These results should be compared to the uncertainty on w of $\pm 0.07(\text{stat}) \pm 0.11(\text{sys})$ reported by K09. Thus neglecting coherent velocities represents a potential systematic error on the best-fit value of w of up to about 2%, or about 13% of the current estimated systematic error budget.²⁷ When future supernova surveys achieve (supernova only) statistical error bars less than about 2%, this potential systematic error will need to be considered carefully, especially for surveys with many nearby supernovae. Indeed the Carnegie supernova project have already found that the magnitude scatter in their sample of $z < 0.08$ supernovae is limited by peculiar velocities (see Folatelli et al. 2010, Fig. 19).

Figure 9 shows the effect of implementing a range of different low-redshift cutoffs on the supernova data, both for the original K09 MLC2k2 data (solid lines) and for our version of that data with uncertainties corrected for correlated motion (dashed lines).²⁸ We plot the best fit value of w derived for a flat model with w and Ω_m as

²⁷ Adding 0.014 to the systematic error budget represents an increase of 13% over the current 0.11 systematic uncertainty estimate.

²⁸ Note that K09 also uses the SALT II light-curve fitter and the results differ. We do not debate the merits of different light-curve fitters here, our qualitative results are relevant whichever light-curve fitter is used.

free parameters.

The correlation-corrected result (dashed line) can be matched by implementing a larger low- z cut on the uncorrected data (e.g. the correlation-corrected result with $z_{\text{cut}} \approx 0.015$ matches the uncorrected data with $z_{\text{cut}} \approx 0.017$). It is also evident that the effect of the low- z cut on the data with correlated errors is smaller than on the data set with uncorrelated errors. Both of these features are as expected, because some of the low- z cut was already effectively implemented by the down-weighting due to correlations. We also note that the SDSS supernovae are much less prone to correlations than the Nearby sample, simply due to their greater distance. SDSS supernova therefore provide a larger improvement to the low-redshift anchor of the magnitude-redshift diagram than one might naïvely expect.

This analysis demonstrates that if the velocity covariance matrix had been used in K09 then the need for a low- z cut would have been diminished. Using the covariance matrix for the peculiar velocity uncertainties should be an optimal statistical treatment of the supernova data. It automatically includes the effect of monopole uncertainties and dipole uncertainties as well as the higher-order correlated motions. Although slightly more complicated to implement than a simple low- z cut, the results are more robust. (This can be seen by the smaller slope of the correlation-corrected analysis vs redshift cut in Fig. 9).

Computing the full correlation matrix does have some disadvantages, primarily because it is model dependent. Our calculation of correlations has been made in a fiducial Λ CDM model, so it is not strictly self-consistent to use these correlations to test other models. However, this is mitigated by the fact that the majority of the covariance signal comes from low redshifts, and most viable models for the universe have to agree fairly closely on the evolution and growth of structure in the local universe in order to match observations. To check the differences are negligible the correlations can be self-consistently re-derived for each cosmological being fitted.

As future surveys with many more supernovae attempt to obtain percent-level accuracy on the value of the equation of state the effect of correlations will become ever more important. At the very least, neglecting correlations under-estimates the *uncertainty* on our cosmological inferences, and in the worst-case scenario can bias the values of cosmological parameters we derive.

4. LOCAL UNDER- OR OVER-DENSITY

In cosmology the monopole term describes the expansion as a function of radial distance, r . In an homogeneous universe the monopole is usually described by Hubble's law, in which the velocity of the comoving object is proportional to its distance from the origin, $v(t) = H(t)r$, where $H(t)$ is known as the Hubble parameter.

In an inhomogeneous universe the Hubble parameter can also depend on spatial position, $H(t, r)$. When that spatial dependence is spherically symmetric it contributes an additional factor to the monopole term of the expansion, which is very difficult to detect observationally, because its primary effect is simply to shift the redshift of all objects. It effectively just makes all objects appear more or less distant.

Were an observer to find themselves off-centre within a

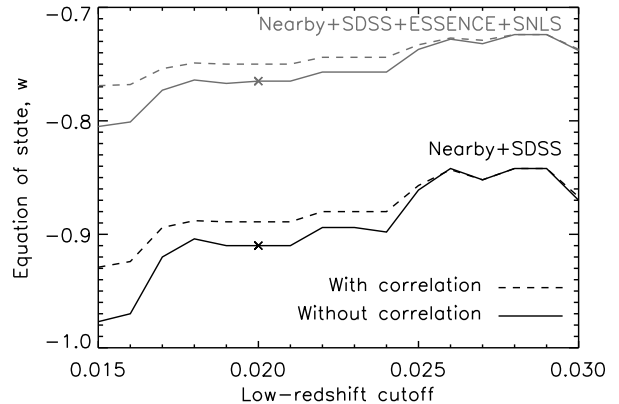


FIG. 9.— Effect of low- z cut on SN data, where the solid lines show the best fit equation of state obtained while neglecting correlated errors and the dashed lines show the same when correlations have been taken into account statistically (model assumes flatness with w and Ω_m the only free parameters, c.f. K09 Fig. 21). The upper and lower sets of lines show how much the results differ when you respectively include or exclude high-redshift data. Upper (grey) curves are for the K09 data set ‘d’, with Nearby, SDSS, ESSENCE, and SNLS supernova samples. Lower (black) curves are for the K09 data set ‘c’, with only the Nearby and SDSS data included. K09 use a low-redshift cutoff of 0.02 (crosses) with systematic uncertainties (calculated for the flat- Λ CDM model with the MLCS light-curve fitter) of ± 0.11 for set ‘d’ and $+0.10 - 0.33$ for set ‘c’ (the greater systematic uncertainty in the lower direction for the set ‘c’ arises primarily due to uncertainties in the rest-frame U band). So the offset seen here between these two data set combinations is within the uncertainties. The effect of correlations is currently smaller than the other systematic uncertainties considered in K09, but will be important for attempts to measure w to better than 3%. Raising the low-redshift cutoff to 0.025 is sufficient to remove the expected effect of correlated supernova motions.

density fluctuation the existence of the fluctuation would be much easier to observe as it would imprint an observational signature akin to the dipole in the CMB. While the induced CMB dipole can always be accommodated by introducing a balancing peculiar velocity of the observer, such a motion simultaneously affects the SN Ia observations. Blomqvist & Mortsell (2009) showed that when considering voids large enough to explain the apparent acceleration of the universe without dark energy, a combined analysis of CMB and supernovae data restricts our position to within 1% of the centre of the density fluctuation.

The potential presence of a monopole term due to a local underdensity is of particular interest to supernova cosmology because the discovery of the acceleration of the universe is founded on the observation that high-redshift type Ia supernovae appear to be more distant than expected in a decelerating universe (Riess et al. 1998; Perlmutter et al. 1999). This observation has incited intense scrutiny of the potential for a local underdensity, known as a “Hubble bubble”, that may be influencing our results.

Zehavi et al. (1998) first reported evidence for a local Hubble bubble in the supernova data, which was refined by Jha et al. (2006) by including more supernovae and by embedding the proposed void in a Λ CDM universe. This reported Hubble bubble corresponds to a local Hubble parameter elevated by approximately 5% relative to the global mean, on scales of the order $70h^{-1}\text{Mpc}$. This

interpretation is reasonable as this distance is roughly the scale of observed large scale structure in our universe (Geller et al. 1997). However, these results have been challenged by papers such as Conley et al. (2007), who show that systematic effects in the treatment of colour terms in the light-curve fitting procedure could be producing a false signal. The evidence for the Hubble bubble is also questioned by other surveys, such as Tully-Fisher and galaxy cluster measurements (e.g. Giovanelli et al. 1999; Hudson et al. 2004), that find no significant local underdensity.

Remarkably a local underdensity can actually mimic the turn-over in the Hubble diagram at high redshift where the universe transitioned from the decelerating phase of the early universe to the accelerating phase we see now (see Fig. 4 of Sollerman et al. 2009). That means that the Hubble Space Telescope observations of supernovae beyond a redshift of $z \sim 1$ (Riess et al. 2004, 2007) that appear closer than expected (in contrast to those at $z \lesssim 1$ that appear further than expected) does not necessarily invalidate the Hubble bubble model.

Many authors (Alnes et al. 2006; Enqvist & Mattsson 2007; Enqvist 2008; García-Bellido & Haugbølle 2008; García-Bellido & Haugbølle 2008, 2009; Zibin et al. 2008; Clifton et al. 2008; Alexander et al. 2009) have studied the size of void required to completely explain away the apparent acceleration in the supernova results. The size required is so vast that the likelihood of us being in such a void in a universe that is on average homogeneous is extremely small. We could abandon the Copernican principle (that we are not in a special place in the universe) and construct a model for our universe in which we do happen to be in such an enormous void. However, the additional restriction that we must be very close to the centre of that void to avoid seeing an excessively large dipole in the CMB, makes such a model very contrived (Alnes & Amarzguioui 2006; Caldwell & Stebbins 2008; Blomqvist & Mortsell 2009).

Nevertheless, the prevailing model of the universe contains a spectrum of density fluctuations, and as observers placed in a random galaxy amongst that distribution we should consider the chance that we are sitting in a small density fluctuation – say one standard deviation away from the mean density – which could possibly have a noticeable effect on the cosmological results we derive.

Here we study the monopole in two ways. First we perform a simulation of large scale structure to predict the distribution of density fluctuations expected in a Λ CDM universe. We can then compare this for consistency with the density fluctuations observed. Secondly we calculate the effect a ‘typical’ density fluctuation has on supernova cosmology, and test whether inserting a low-redshift cut-off in the supernova data can eliminate the effect of local density fluctuations.

4.1. Modelling the size of density fluctuations

Once we have derived a model (such as Λ CDM) from the observational data we can ask whether the density fluctuations predicted in this model are consistent with those observed. We can also address whether our treatment of the dipole is justified and whether it is likely that an undiagnosed monopole term could be biasing our results. This checks the internal consistency of the model as well as testing for biases our assumptions may impose

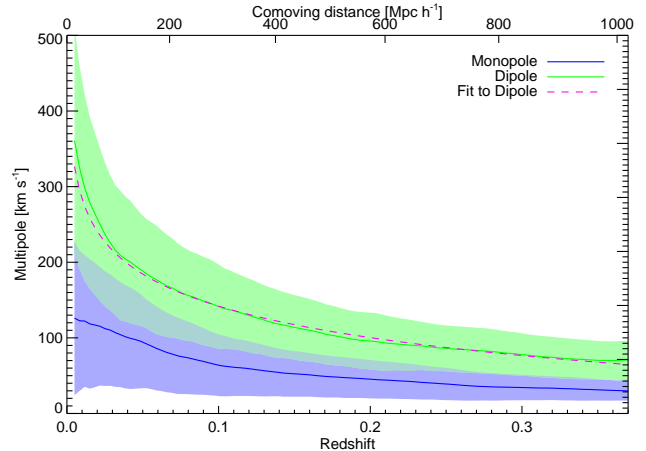


FIG. 10.— The average monopole and dipole in the velocity field as extracted from a large N-body simulation with best-fit WMAP5 cosmological parameters. The shaded areas indicate the cosmic variance. The dashed line is the best-fit model, Eq. (30). See the electronic edition of the Journal for a color version of this figure.

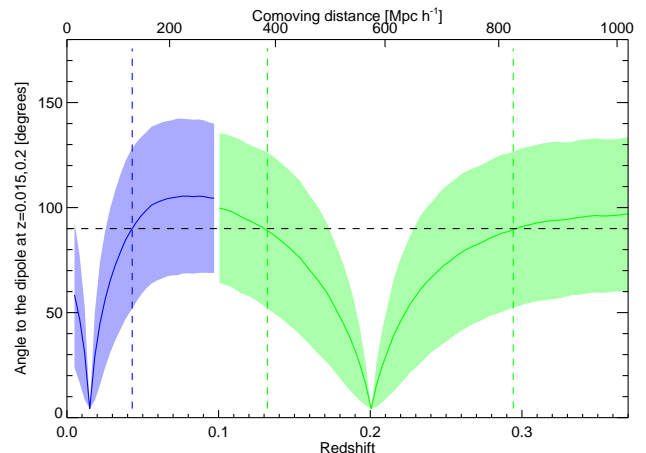


FIG. 11.— To what distance can the direction of the local dipole be extrapolated? This plot shows the relative direction of the dipole as measured by observers at two reference redshifts $z_0 = 0.015, 0.2$ (blue and green respectively). When the change reaches 90° (dashed lines), which occurs at $z_{90}=0.043$ and $z_{90}=\{0.132, 0.294\}$, the dipole to a shell at that radius bears no correlation with the dipole in shells very close to the observer. The shaded area is the cosmic variance. As expected, the size of the region in which the directions of the dipole are aligned increases with redshift, from $\Delta z_{90} \sim 0.03$ to $\Delta z_{90} \sim 0.08$ for the two cases shown here. See the electronic edition of the Journal for a color version of this figure.

on our results.

To this end we have performed a large scale dark matter N-body simulation ($L_{\text{box}}=2048 \text{ Mpc } h^{-1}$, $N_{\text{part}}=1024^3$, $z_{\text{start}}=49$) using the Gadget2 code (Springel 2005) with best-fit WMAP5 cosmological parameters $\{\Omega_m, \Omega_\Lambda, h, w, n_s, \sigma_8\} = \{0.2792, 0.7208, 0.701, -1, 0.96, 0.817\}$, (Komatsu et al. 2009). Using 2000 observers placed at random, but weighted by mass, we have calculated the average magnitude of the monopole and the dipole, together with the cosmic variance of each (see Fig. 10). We define the magnitude of the monopole to be $\sigma(M) = \sqrt{\frac{\pi}{2}} \langle |M| \rangle$, where $\sigma(M)$ is the root-mean-square of the signed monopole, and the signed monopole is simply the mean velocity (either towards or away) of matter in a shell of a particular distance.

While the analysis is done at redshift zero using a single data snapshot, the velocities have been corrected using linear theory, so the velocities in Fig. 10 are in the lightcone. The correction from translating the velocities to the lightcone is minor, at maximum 1%.

In order to calculate the mean size of the dipole and how it varies with distance (redshift) we sliced the resulting simulation into shells with a range of radii between $10 h^{-1}\text{Mpc} < r < 1000 h^{-1}\text{Mpc}$ around each of the random observers. We then measured the mean motion of these shells to calculate the monopole and dipole the central observer would see for sources at that distance.

We have done the analysis both with shells with a thickness of $10 h^{-1}\text{Mpc}$ and of $1 h^{-1}\text{Mpc}$, and confirmed that the results do not depend on the shell thickness, except at the very lowest redshifts where the thickness becomes comparable to the radius of the shell. The magnitude of the dipole is reasonably well described by the simple model

$$v_d = (507 \pm 51) - (65 \pm 8) \ln \left(\frac{R_0 \chi}{1 \text{Mpc } h^{-1}} \right) \text{ km s}^{-1}, \quad (30)$$

$$= (-8 \pm 12) - (63 \pm 7) \ln(z) \text{ km s}^{-1},$$

where the differences in the fits using either comoving distance ($R_0 \chi$) or redshifts are due to the slightly non-linear conversion between the two at larger distances.

The mean magnitude of the dipole at low redshifts ($z \sim 0.01$) is approximately $300 \pm 100 \text{ km s}^{-1}$. This is consistent with the average random peculiar velocity uncertainty we assume for supernovae.

The mean absolute magnitude of the monopole, which is also plotted in Fig. 10, is smaller than the dipole but still significant, on the order of 100 km s^{-1} . We investigate in Section 4.2 the impact this mean monopole would have on our cosmological inferences.

The direction of the dipole of the local velocity field is only known at very low redshifts. To test how well this knowledge can be extrapolated to higher redshifts, Fig. 11 shows how the direction of the dipole in the simulation changes as a function of redshift. The direction is measured with respect to the direction of the dipole at two reference redshifts $z = 0.015, 0.2$. These redshifts correspond respectively to the redshift of the currently available local dipole measurement, and a redshift representative of the SDSS supernovae.

A naïve expectation would be that the average local dipole should decrease with redshift until we reach sources that are too distant to share any significant common source of gravitational attraction with us. At that point the sources should be on-average at rest with respect to the CMB, and therefore our dipole direction with respect to those sources, if we do not correct for our local velocity, should be simply the direction of the CMB dipole. When we do correct for the local velocity (as done in Figure 11), while the amplitude of the local dipole decreases, the direction still changes at higher redshifts, and it only makes sense to extrapolate the currently known dipole direction out to $z \approx 0.045$.

This result is interesting seen in light of observational results pointing towards a coherent dipole direction out to at least $300 h^{-1}\text{Mpc}$ (i.e. $z \sim 0.1$, Kashlinsky et al. 2008), since not only the magnitude of the observed

dipole velocity ($1600 \pm 500 \text{ km s}^{-1}$ at $z \sim 0.03$ and $850 \pm 250 \text{ km s}^{-1}$ at $z \sim 0.1$) but also the constancy of the the direction of the dipole is surprising ($\sim 3\sigma$ deviation) when interpreted in the framework of the ΛCDM cosmology.

4.2. The impact of density fluctuations on SN cosmology

We now extend this study to analyse the effect a *typical* local density fluctuation has on cosmological parameter estimation with supernovae. In Sinclair et al. (2010) some of the current authors examined this effect in general. Here we summarise the Sinclair et al. (2010) results and relate them to the SDSS data specifically.

Sinclair et al. (2010) used the Lemaître-Tolman-Bondi (LTB) model to simulate a local underdensity, as outlined in Garcia-Bellido & Haugbølle (2008). By adapting their LTB software²⁹ we generated model magnitude-redshift data for a Hubble bubble universe with a Gaussian void profile that follows a radial matter density profile of,

$$\Omega_M(r) = \Omega_M^{\text{out}} [1 - \delta e^{(-r/r_0)^2}], \quad (31)$$

where r_0 is the characteristic void radius and the density contrast is defined as $\delta = (\Omega_M^{\text{out}} - \Omega_M^{\text{in}})/\Omega_M^{\text{out}}$. We then fit these data with a model (ΛCDM) that erroneously assumes the simulated universe is homogeneous and compare the parameters so derived with the parameters input into the simulation.

We chose to test a void (underdensity) of $r_0 = 70 h^{-1}\text{Mpc}$, with $\delta = -0.3$, corresponding to a maximal monopole velocity of 120 km s^{-1} . This is a reasonable size void given the statistical distribution derived in the previous section. This model is of further interest because it is the radius of Hubble bubble suggested by the supernova data (Jha et al. 2006; see however Conley et al. 2007), and is also close to the observed scale of structures in our universe (Geller & Huchra 1989; Geller et al. 1997; Hoyle & Vogeley 2004).

We simulated this underdensity embedded in a ΛCDM universe with $(\Omega_M, \Omega_\Lambda) = (0.3, 0.7)$. Specifically, we generated a set of ideal magnitude-redshift data points (301 points evenly distributed over $0 < z < 1.7$) exactly matching the void model, and gave these distance modulus uncertainties of 0.2 mag . We test how badly such an underdensity would bias our cosmological conclusions by fitting an homogeneous model to this local underdensity+ ΛCDM data. If the void has no impact we expect to recover $(\Omega_M, \Omega_\Lambda) = (0.3, 0.7)$. Anything else represents a systematic offset caused by the local underdensity that will not be mitigated by adding more data.

A similar technique was used by Vanderveld (2008) to study the effect of peculiar velocities on supernova cosmology, taking the distribution of peculiar velocities from an N -body simulation. They found that $z_{\text{cut}} = 0.02$ was the optimal low-redshift cutoff but applying it only reduced the error in the cosmological parameters by about 10%. Below we find that if we happen to live in one of the low density regions of the universe and consider the gravitational redshift that would induce, then the low-redshift cut could be of greater importance.

²⁹ <http://www.phys.au.dk/~haugboel/software.shtml>

Upon fitting a homogeneous model to our Λ CDM+void data we extracted best-fit parameters $(\Omega_M, \Omega_\Lambda) = (0.299, 0.73)$, corresponding to a 0.3% discrepancy in the matter density and a 4% discrepancy in the cosmological constant density, compared to the input parameters. This size of discrepancy is not insignificant, given the current uncertainty in cosmological parameters: the WMAP results in Komatsu et al. (2009) cite a 2% uncertainty on the best fit value of the cosmological constant.

This analysis demonstrates the importance of implementing a low-redshift cutoff. The above discrepancies in Ω_M and Ω_Λ are reduced to 0.06% and 1% respectively when a low-redshift cut of $z_{\text{cut}} = 0.02$ is used.

The discrepancies become more severe (but with larger uncertainties) when we allow the equation of state of dark energy to differ from $w = -1$ during the fit. Starting with a simulation with $(\Omega_M, \Omega_\Lambda, w) = (0.3, 0.7, -1.0)$, when we simultaneously fit the three parameters in the presence of the void we get a discrepancy in w of 44% with no low- z cut, which is reduced to a discrepancy of 8.5% when using $z_{\text{cut}} = 0.02$. Imposing flatness reduces the discrepancies without and with the low- z cut to 7% and 1.4% respectively. (Without a low-redshift cutoff the best fit models are $(\Omega_M, \Omega_\Lambda, w) = (0.31, 0.54, -1.4)$ when curvature is permitted, and $(\Omega_M, w) = (0.30, -1.07)$ when flatness is imposed.)

We emphasise that this analysis is only hypothetical — *if* we live in a 30% underdensity of scale $70h^{-1}\text{Mpc}$, *then* assuming the universe is homogeneous could dupe us into believing that w is far more phantom-like (< -1), and the density of dark energy far more significant, than they really are.

Even though the proposed void is only hypothetical, given that these discrepancies remain significant it is worth investigating the potential impact on recent data sets and whether a higher low- z cutoff might be worthwhile.

To that end we here apply the Sinclair et al. (2010) result to the SDSS data explicitly. At each observed redshift we alter the SDSS data for the effects of a hypothetical void of the type described above ($r_0 = 70h^{-1}\text{Mpc}$, with $\delta = -0.3$). The difference is shown in the upper panel of Fig. 12, in which the standard low- z cut of $z_{\text{cut}} = 0.02$ has been used. This low-redshift cutoff is motivated empirically not only because random peculiar velocities are significant below that redshift, but also because for $z_{\text{cut}} < 0.02$ the best fit parameters depend strongly on the choice of z_{cut} (see Sect. 9.1 and Fig. 21 of K09).

Although in Fig. 12 there appears to be a large shift in the best fit parameters, from $(\Omega_m, w_0) = (0.40, -1.00)$ to $(0.37, -0.86)$, the final cosmological parameters are not susceptible to this full discrepancy because most of the variation is along the long-axis of the contours, which is well constrained by other observations such as the CMB and BAO. The direction that the supernovae constrain most tightly is only changed a very small amount by the presence of a local void.

It could nevertheless be argued that a higher low- z cutoff may be necessary to avoid the effects of local inhomogeneities. However, by excluding low redshift data one sacrifices constraining power. In the lower panel of Fig. 12 we show the result of increasing the low- z cutoff to $z_{\text{cut}} = 0.04$. Although the effect of the void is now

negligible (shaded and black contours overlap) the contours have shifted further due to the loss of constraining power than they did due to the hypothetical void. We therefore conclude that increasing the redshift cutoff is counter-productive with the size of the low- z SN sample used in K09.

This could be considered another argument for using the covariance matrix approach to down-weighting low- z supernovae since it automatically takes into account potential monopole velocities.

5. CONCLUSIONS

From this study we can conclude that the cosmological results derived by the SDSS SN survey are robust to peculiar velocity systematics. The local dipole represents a negligible addition to the CMB dipole correction that has already been implemented, but future surveys with many nearby supernovae may need to take it into account. An isotropically distributed local supernova sample would shield us, to a great extent, from systematic errors due to the local dipole.

Neglecting correlated peculiar velocities can cause an error in the best-fit value of w , which in the current sample underestimates w by about 2%, and causes us to overestimate the precision of our measurement. As future surveys aim for percent-level accuracy on the value of the equation of state, the importance of correlations between the peculiar velocities of supernovae will increase. Here we treated them in a statistical sense, but it may be possible in the future to correct the supernova velocities for measured local flows. A future method of testing cosmological parameters will be to use the peculiar velocities as signal rather than noise, and generate a peculiar velocity power spectrum to compare against cosmological models. In the meantime, we find that accounting for peculiar velocities by using a covariance matrix for the correlated errors is a more robust way to down-weight low-redshift supernovae than applying a sharp low-redshift cut. Doing so does not degrade the uncertainties in w , despite the down-weighting of the signal, because one can include more low-redshift supernovae in the overall fit.

Finally, we used n -body simulations to gauge the likely distribution of local under- and over-densities and found that a density fluctuation of 30% from the mean cosmological density, out to a range of $70h^{-1}\text{Mpc}$, is reasonable given the expectations of concordance Λ CDM. A density fluctuation of this size can have a significant impact on the cosmological parameters we derive. It is crucial to implement a low-redshift cut-off to escape the worst of those systematic errors and we demonstrated that the currently used $z_{\text{cut}} = 0.02$ is well justified. However, we advocate including the velocity covariance directly in one's likelihood analysis as a more systematic way to down-weight the low z SNe.

In conclusion, the local dipole, coherent motions, and local density fluctuations, all have systematic effects on supernova cosmology. Although these are negligible for current data sets we have shown how to correct for them when they become more significant for larger data sets of the future.

TMD thanks Alexandra Abate for useful comments and also the Centro de Ciencias de Bensque Pedro Pas-

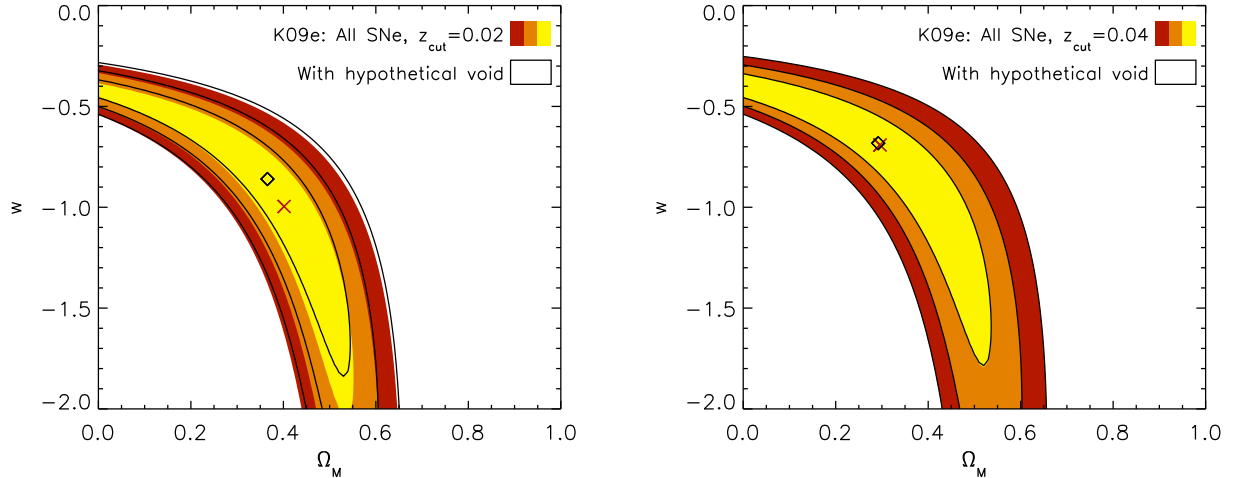


FIG. 12.— This figure demonstrates the effect of correcting the SN data for a hypothetical ‘Hubble Bubble’, in this case a Gaussian underdensity of 30% on a scale of $70h^{-1}\text{Mpc}$. In the upper panel the shaded contours display the K09 data set e (with the maximum likelihood indicated by the red cross) and black outline indicates the results for the same data corrected for a local void (with the maximum likelihood indicated by a black diamond). In the upper panel the low-redshift cutoff was the standard $z_{\text{cut}} = 0.02$. The lower panel demonstrates the effect of increasing the low-redshift cutoff from $z_{\text{cut}} = 0.02$ to $z_{\text{cut}} = 0.04$. The analysis is identical to the upper panel except that in both the homogeneous case (shaded contours) and the putative ‘Hubble bubble’ case (black outline), the low-redshift cutoff was $z_{\text{cut}} = 0.04$. Although increasing the low-redshift cut reduces the susceptibility of the data to local density fluctuations, dropping the low-redshift data changes the best fit cosmology by more than the local void would because of the weakened constraints. See also how the best fit w changes with changing low- z cut in Fig. 9. See the electronic edition of the Journal for a color version of this figure.

cual for providing us with such a superb facility during some of the work on leading to this paper.

Computer time was provided by the Danish Center for Scientific Computing (DCSC). Some of the results in this paper have been derived using the HEALPix³⁰ (Górski et al. 2005) package.

Funding for the SDSS and SDSS-II has been provided by the Alfred P. Sloan Foundation, the Participating Institutions, the National Science Foundation, the U.S. Department of Energy, the National Aeronautics and Space Administration, the Japanese Monbukagakusho, the Max Planck Society, and the Higher Education Funding Council for England. The SDSS Web Site is <http://www.sdss.org/>.

The SDSS is managed by the Astrophysical Research Consortium for the Participating Institutions. The Participating Institutions are the American Museum of Natural History, Astrophysical Institute Potsdam, University of Basel, University of Cambridge, Case Western Reserve University, University of Chicago, Drexel University, Fermilab, the Institute for Advanced Study, the Japan Participation Group, Johns Hopkins University, the Joint Institute for Nuclear Astrophysics, the Kavli Institute for Particle Astrophysics and Cosmology, the Korean Scientist Group, the Chinese Academy of Sciences (LAMOST), Los Alamos National Laboratory, the Max-Planck-Institute for Astronomy (MPIA), the Max-Planck-Institute for Astrophysics (MPA), New Mexico State University, Ohio State University, University of Pittsburgh, University of Portsmouth, Princeton University, the United States Naval Observatory, and the

University of Washington.

This work is based in part on observations made at the following telescopes. The Hobby-Eberly Telescope (HET) is a joint project of the University of Texas at Austin, the Pennsylvania State University, Stanford University, Ludwig-Maximilians-Universität München, and Georg-August-Universität Göttingen. The HET is named in honor of its principal benefactors, William P. Hobby and Robert E. Eberly. The Marcario Low-Resolution Spectrograph is named for Mike Marcario of High Lonesome Optics, who fabricated several optical elements for the instrument but died before its completion; it is a joint project of the Hobby-Eberly Telescope partnership and the Instituto de Astronomía de la Universidad Nacional Autónoma de México. The Apache Point Observatory 3.5 m telescope is owned and operated by the Astrophysical Research Consortium. We thank the observatory director, Suzanne Hawley, and site manager, Bruce Gillespie, for their support of this project. The Subaru Telescope is operated by the National Astronomical Observatory of Japan. The William Herschel Telescope is operated by the Isaac Newton Group on the island of La Palma in the Spanish Observatorio del Roque de los Muchachos of the Instituto de Astrofísica de Canarias. The W.M. Keck Observatory is operated as a scientific partnership among the California Institute of Technology, the University of California, and the National Aeronautics and Space Administration. The Observatory was made possible by the generous financial support of the W. M. Keck Foundation.

Facilities: Nickel, HST (STIS), CXO (ASIS).

APPENDIX

APPENDIX A: TREATMENT OF RANDOM PECULIAR VELOCITY CONTRIBUTIONS

The motion of distant supernovae and their host galaxies imprints a peculiar velocity error that is primarily random (as opposed to our own motion, on which Sect. 2 concentrates). That peculiar velocity dispersion $\sigma_p^{\text{pec}} \sim 300\text{km s}^{-1}$

³⁰ <http://healpix.jpl.nasa.gov>

gives a redshift error of $\sigma_z^{\text{pec}} = \sigma_v^{\text{pec}}/c$ (or the special relativistic formula if the peculiar velocity was higher). The measured redshift, z , is a combination of the recession and peculiar velocity contributions according to $(1+z) = (1+\bar{z})(1+z^{\text{pec}})$, where \bar{z} and z^{pec} are the recession and peculiar velocity contributions to the redshift, respectively. Differentiating this expression to calculate the error contribution from peculiar velocities gives

$$\sigma_z = (1+\bar{z})\sigma_z^{\text{pec}} + (1+z^{\text{pec}})\sigma_{\bar{z}}. \quad (\text{A1})$$

We can take the error in recession velocity to be zero, $\sigma_{\bar{z}} = 0$, so the uncertainty we need to add to our redshifts to account for peculiar velocities is $\sigma_z = (1+\bar{z})\sigma_z^{\text{pec}}$.

Previous analyses, including for example Davis et al. (2007), used $\sigma_z = \sigma_z^{\text{pec}}$ and so slightly underestimated the contribution from peculiar velocities at high redshifts. Formally, the uncertainty at $z = 1$ should have been double what was used, but since the proportional contribution from peculiar velocities still decreases with redshift, this only corresponds to an error of 0.26%, as opposed to 0.13%, and the difference is negligible for cosmology.

We convert σ_z into an approximate magnitude uncertainty, σ_m^{pec} , using the magnitude-redshift relation, and combine it in quadrature with the uncertainty in the measured magnitude, σ_m^{meas} , and the intrinsic magnitude dispersion, σ_m^{int} , of the supernovae.

The distance modulus has the form

$$\mu = 5 \log_{10}(\bar{d}_L) = \frac{5}{\ln(10)} \ln[\tilde{\chi}(1+\bar{z})], \quad (\text{A2})$$

where $\tilde{\chi} = R_0\chi = c \int_0^{\bar{z}} H(z)^{-1} dz$ is the comoving distance. Therefore an error in the redshift corresponds to a magnitude error of

$$\sigma_\mu = \sigma_z \frac{5}{\ln(10)} \left[\frac{1}{1+\bar{z}} + \frac{c}{\tilde{\chi}H(\bar{z})} \right]. \quad (\text{A3})$$

Although a fiducial cosmology is used for this calculation – often taken to be Λ CDM with $\Omega_M \sim 0.3$ and $\Omega_\Lambda \sim 0.7$ – differences from the derived cosmology are small and have negligible impact on cosmology fits. Note that K09 use the empty universe as their fiducial cosmology for error calculations, and approximate the empty universe case, in which $H(\bar{z}) = H_0(1+\bar{z})$ and $\tilde{\chi} = c \ln(1+\bar{z})/H_0$, by

$$\sigma_\mu \sim \sigma_z \frac{5}{\ln(10)} \left[\frac{1+\bar{z}}{\bar{z}(1+\bar{z}/2)} \right]. \quad (\text{A4})$$

The difference between this approximation and Eq. A3 is shown in Fig. 13.

In the non-flat case $\tilde{\chi}$ should be replaced with $R_0 S_k(\chi)$ in the equation for μ , or $R_0 T_k(\chi)$ in the equation for σ_μ , where $S_k = \sin$ or \sinh in the closed and open cases, respectively, and $T_k = \tan$ or \tanh .

APPENDIX B: THE EQUIVALENCE OF THE OBSERVER-CENTRIC AND SEPARATION-CENTRIC EXPRESSIONS FOR THE MAGNITUDE COVARIANCE MATRIX

Here we derive the expressions for C_{12}^{vel} in Eq. 28 and 29. These derivations are valid in the flat universe case. It comes down to evaluating the two point velocity correlation $\xi_{12}^{\text{vel}} \equiv \langle (\mathbf{v}_1 \cdot \hat{\mathbf{x}}_1)(\mathbf{v}_2 \cdot \hat{\mathbf{x}}_2) \rangle$, where 1 and 2 label the two SNe in question, since

$$C_{12}^{\text{vel}} = \left[\frac{5}{c \ln 10} \right]^2 \left[1 - \frac{a_1}{a'_1} \frac{c}{\tilde{\chi}_1} \right] \left[1 - \frac{a_2}{a'_2} \frac{c}{\tilde{\chi}_2} \right] \xi_{12}^{\text{vel}}. \quad (\text{B1})$$

This is actually an old subject (see e.g. Gorski 1988). One reason we go over the derivation here is that errors have crept into some recent literature, as pointed out by Gordon et al. (2007). It is also useful to see how two completely different looking expressions, i.e. Eq. 28 and 29, are actually equivalent. Errors have occurred in some recent versions of Eq. 28 (e.g. Hernández-Monteagudo et al. 2006; Cooray & Caldwell 2006).

Using linear theory, it can be shown that

$$\xi_{12}^{\text{vel}} = D'_1 D'_2 \int \frac{d^3 k}{(2\pi)^3} k^{-2} P(k)_{z=0} (\hat{\mathbf{k}} \cdot \hat{\mathbf{x}}_1)(\hat{\mathbf{k}} \cdot \hat{\mathbf{x}}_2) e^{-i\mathbf{k} \cdot (\mathbf{x}_1 - \mathbf{x}_2)} \quad (\text{B2})$$

where \mathbf{x}_1 and \mathbf{x}_2 are the comoving positions of the two SNe in question, $\hat{\mathbf{x}}_1$ and $\hat{\mathbf{x}}_2$ are the unit vectors pointing in these directions, $P(k)_{z=0}$ is the mass power spectrum today, and D'_1 and D'_2 are the derivatives of the growth factor with respect to conformal time at the two redshifts of interest.

An observer-centric approach is to use

$$\hat{\mathbf{k}} \cdot \hat{\mathbf{x}}_2 e^{i\mathbf{k} \cdot \mathbf{x}_2} = 4\pi \sum_{\ell, m} i^{\ell-1} j'_\ell(k\tilde{\chi}_2) Y_{\ell m}^*(\hat{\mathbf{k}}) Y_{\ell m}(\hat{\mathbf{x}}_2) \quad (\text{B3})$$

where j_ℓ is the spherical Bessel function, j'_ℓ is its derivative (with respect to its argument, not conformal time), and $Y_{\ell m}$'s are the spherical harmonics. Performing the integral over $\hat{\mathbf{k}}$ in Eq. B2, and using $\int d\Omega_k Y_{\ell m}^*(\hat{\mathbf{k}}) Y_{\ell' m'}(\hat{\mathbf{k}}) = \delta_{\ell\ell'} \delta_{mm'}$

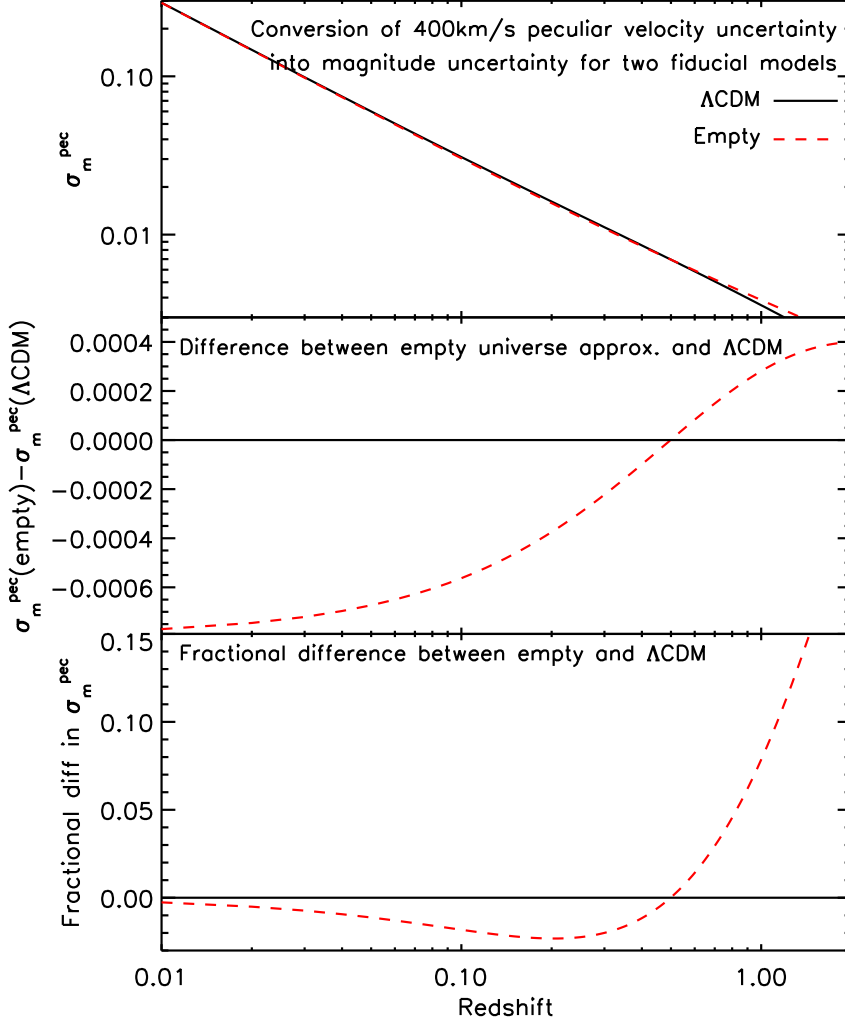


FIG. 13.— Examples of the conversion from redshift uncertainty to magnitude uncertainty. A peculiar velocity uncertainty of $\sigma_v^{\text{pec}} = 300 \text{ km s}^{-1}$ corresponds to $\sigma_z^{\text{pec}} = 0.001$. This value converts to a large magnitude uncertainty at low redshift, where the slope of the magnitude-redshift diagram is steep, but a smaller magnitude uncertainty at high redshift. Different fiducial models give slightly different conversions between redshift and magnitude uncertainties, but the difference is negligible for cosmological inferences. Here the empty model conversion (Eq. A4) is compared to the ΛCDM model conversion (Eq. A3 with $\Omega_m = 0.3$, $\Omega_\Lambda = 0.7$). In absolute terms (middle panel) the difference is largest at low redshift, but in relative terms (lower panel) the difference is largest at high redshifts. The lower panel shows $[\sigma_m^{\text{pec}(\text{empty})} - \sigma_m^{\text{pec}(\Lambda\text{CDM})}] / \sigma_m^{\text{pec}(\Lambda\text{CDM})}$. See the electronic edition of the Journal for a color version of this figure.

and $\mathcal{P}_\ell(\hat{\mathbf{x}}_1 \cdot \hat{\mathbf{x}}_2) = 4\pi/(2\ell + 1) \sum_m Y_{\ell m}^*(\hat{\mathbf{x}}_1) Y_{\ell m}(\hat{\mathbf{x}}_2)$, it is straightforward to show that

$$\xi_{12}^{\text{vel}} = D'_1 D'_2 \int \frac{dk}{2\pi^2} P(k)_{z=0} \sum_\ell (2\ell + 1) j'_\ell(k\tilde{\chi}_1) j'_\ell(k\tilde{\chi}_2) \mathcal{P}_\ell(\hat{\mathbf{x}}_1 \cdot \hat{\mathbf{x}}_2) \quad (\text{B4})$$

from which Eq. 28 can be obtained (see Hui & Greene 2006, for details). The above expression is observer-centric in the sense that one can easily read off from it the angular velocity power spectrum as seen by the observer,

$$C_\ell^{\text{vel}} = D'_1 D'_2 \int \frac{2dk}{\pi} P(k)_{z=0} j'_\ell(k\tilde{\chi}_1) j'_\ell(k\tilde{\chi}_2). \quad (\text{B5})$$

Here, 1 and 2 can refer to the same redshift, or two different redshifts.

A different approach to reducing Eq. B2 is to first note that by symmetry arguments (Gorski 1988),

$$\langle v_i(\mathbf{x}_1) v_j(\mathbf{x}_2) \rangle = [\Pi(r) - \Sigma(r)] \hat{r}_i \hat{r}_j + \Sigma(r) \delta_{ij}, \quad (\text{B6})$$

where i and j here, unlike in the rest of the paper, label the spatial directions rather than the SNe, r is the comoving separation between points 1 and 2, and $\hat{\mathbf{r}}$ is the associated unit vector. Suppose $\hat{\mathbf{r}}$ points in the z direction, then the above matrix is diagonal, with diagonal entries Σ, Σ, Π i.e. Σ is the perpendicular velocity correlation and Π is the parallel velocity correlation. Here, parallel and perpendicular are defined by the separation vector between the two SNe (hence a separation-centric approach). From this matrix, one can deduce that

$$\xi_{12}^{\text{vel}} = (\hat{\mathbf{x}}_1 \cdot \hat{\mathbf{r}})(\hat{\mathbf{x}}_2 \cdot \hat{\mathbf{r}}) \Pi(r) + [\hat{\mathbf{x}}_1 \cdot \hat{\mathbf{x}}_2 - (\hat{\mathbf{x}}_1 \cdot \hat{\mathbf{r}})(\hat{\mathbf{x}}_2 \cdot \hat{\mathbf{r}})] \Sigma(r) \quad (\text{B7})$$

where $[\hat{\mathbf{x}}_1 \cdot \hat{\mathbf{x}}_2 - (\hat{\mathbf{x}}_1 \cdot \hat{\mathbf{r}})(\hat{\mathbf{x}}_2 \cdot \hat{\mathbf{r}})]$ can be written as $\sin\theta_1 \sin\theta_2$ if $\hat{\mathbf{x}}_1 \cdot \hat{\mathbf{r}} = \cos\theta_1$ and $\hat{\mathbf{x}}_2 \cdot \hat{\mathbf{r}} = \cos\theta_2$. Comparing this

expression with Eq. B2, one can see that,

$$\Pi(r) = D'_1 D'_2 \int \frac{d^3 k}{(2\pi)^3} k^{-2} P(k)_{z=0} (\hat{\mathbf{k}} \cdot \hat{\mathbf{r}})^2 e^{i\mathbf{k} \cdot \mathbf{r}}. \quad (\text{B8})$$

Using

$$e^{i\mathbf{k} \cdot \mathbf{r}} = \sum_{\ell} (2\ell + 1) i^{\ell} j_{\ell}(kr) \mathcal{P}_{\ell}(\hat{\mathbf{k}} \cdot \hat{\mathbf{r}}) \quad (\text{B9})$$

and integrating over $\hat{\mathbf{k}}$ (choosing $\hat{\mathbf{r}}$ to lie in the z direction for instance), one can see that only $\ell = 2$ and $\ell = 0$ survives. Finally, using $j_2 = 3j_1/x - j_0$, one obtains,

$$\Pi(r) = D'_1 D'_2 \int \frac{dk}{2\pi^2} P(k)_{z=0} \left[j_0(kr) - \frac{2j_1(kr)}{kr} \right]. \quad (\text{B10})$$

The perpendicular counterpart can be similarly obtained from,

$$\Sigma(r) = D'_1 D'_2 \int \frac{d^3 k}{(2\pi)^3} \frac{P(k)_{z=0}}{k^2} (\hat{\mathbf{k}} \cdot \hat{\mathbf{x}})^2 e^{i\mathbf{k} \cdot \mathbf{r}}, \quad (\text{B11})$$

with $\hat{\mathbf{x}}$ pointing in the x direction while $\hat{\mathbf{r}}$ points in the z direction. A few manipulations yield,

$$\Sigma(r) = D'_1 D'_2 \int \frac{dk}{2\pi^2} P(k)_{z=0} \frac{j_1(kr)}{kr}, \quad (\text{B12})$$

reproducing the results of Gorski (1988) and giving our Eq. 29.

REFERENCES

- Abate, A., & Lahav, O. 2008, *MNRAS*, 389, L47
- Alexander, S., Biswas, T., Notari, A., & Vaid, D. 2009, *Journal of Cosmology and Astro-Particle Physics*, 9, 25
- Alnes, H., & Amarzguoui, M. 2006, *Phys. Rev. D*, 74, 103520
- Alnes, H., Amarzguoui, M., & Grøn, Ø. 2006, *Phys. Rev. D*, 73, 083519
- Astier, P. et al. 2006, *A&A*, 447, 31
- Bennett, C. L. et al. 2003, *ApJS*, 148, 1
- Blomqvist, M., & Mortsell, E. 2009, *ArXiv e-prints*
- Bonvin, C., Durrer, R., & Gasparini, M. A. 2006a, *Phys. Rev. D*, 73, 023523
- Bonvin, C., Durrer, R., & Kunz, M. 2006b, *Physical Review Letters*, 96, 191302
- Caldwell, R. R., & Stebbins, A. 2008, *Physical Review Letters*, 100, 191302
- Clifton, T., Ferreira, P. G., & Land, K. 2008, *Physical Review Letters*, 101, 131302
- Conley, A., Carlberg, R. G., Guy, J., Howell, D. A., Jha, S., Riess, A. G., & Sullivan, M. 2007, *ApJ*, 664, L13
- Cooray, A., & Caldwell, R. R. 2006, *Phys. Rev. D*, 73, 103002
- Croton, D. J. et al. 2004, *MNRAS*, 352, 828
- Davis, T. M., & Lineweaver, C. H. 2004, *Publications of the Astronomical Society of Australia*, 21, 97
- . 2005, *Scientific American*, 292, 36
- Davis, T. M. et al. 2007, *ApJ*, 666, 716
- Eisenstein, D. J. et al. 2005, *ApJ*, 633, 560
- Enqvist, K. 2008, *General Relativity and Gravitation*, 40, 451
- Enqvist, K., & Mattsson, T. 2007, *Journal of Cosmology and Astro-Particle Physics*, 2, 19
- Erdoğan, P. et al. 2006, *MNRAS*, 368, 1515
- Folatelli, G. et al. 2010, *AJ*, 139, 120
- Freedman, W. L. et al. 2009, *ApJ*, 704, 1036
- Frieman, J. A. et al. 2008, *AJ*, 135, 338
- Furlanetto, S. R., & Piran, T. 2006, *MNRAS*, 366, 467
- García-Bellido, J., & Haugbølle, T. 2008, *Journal of Cosmology and Astro-Particle Physics*, 4, 3
- García-Bellido, J., & Haugbølle, T. 2008, *Journal of Cosmology and Astro-Particle Physics*, 9, 16
- . 2009, *Journal of Cosmology and Astro-Particle Physics*, 9, 28
- Geller, M. J., & Huchra, J. P. 1989, *Science*, 246, 897
- Geller, M. J. et al. 1997, *AJ*, 114, 2205
- Giovanelli, R., Dale, D. A., Haynes, M. P., Hardy, E., & Campusano, L. E. 1999, *ApJ*, 525, 25
- Gordon, C., Land, K., & Slosar, A. 2007, *Physical Review Letters*, 99, 081301
- . 2008, *MNRAS*, 387, 371
- Gorski, K. 1988, *ApJ*, 332, L7
- Górski, K. M., Hivon, E., Banday, A. J., Wandelt, B. D., Hansen, F. K., Reinecke, M., & Bartelmann, M. 2005, *ApJ*, 622, 759
- Hamuy, M. et al. 1996, *AJ*, 112, 2408
- Hannestad, S., Haugbølle, T., & Thomsen, B. 2008, *Journal of Cosmology and Astro-Particle Physics*, 2, 22
- Haugbølle, T., Hannestad, S., Thomsen, B., Fynbo, J., Sollerman, J., & Jha, S. 2007, *ApJ*, 661, 650
- Hernández-Monteagudo, C., Verde, L., Jimenez, R., & Spergel, D. N. 2006, *ApJ*, 643, 598
- Hicken, M., Wood-Vasey, W. M., Blondin, S., Challis, P., Jha, S., Kelly, P. L., Rest, A., & Kirshner, R. P. 2009, *ApJ*, 700, 1097
- Holtzman, J. A. et al. 2008, *AJ*, 136, 2306
- Hoyle, F., & Vogeley, M. S. 2004, *ApJ*, 607, 751
- Hudson, M. J., Smith, R. J., Lucey, J. R., & Branchini, E. 2004, *MNRAS*, 352, 61
- Hui, L., & Greene, P. B. 2006, *Phys. Rev. D*, 73, 123526
- Jha, S. et al. 2006, *AJ*, 131, 527
- Jha, S., Riess, A. G., & Kirshner, R. P. 2007, *ApJ*, 659, 122
- Kashlinsky, A., Atrio-Barandela, F., Kocevski, D., & Ebeling, H. 2008, *ApJ*, 686, L49
- . 2009, *ApJ*, 691, 1479
- Kessler, R. et al. 2009, *ApJS*, 185, 32
- Kogut, A. et al. 1993, *ApJ*, 419, 1
- Komatsu, E. et al. 2009, *ApJS*, 180, 330
- . 2010, *ArXiv e-prints*
- Kowalski, M. et al. 2008, *ApJ*, 686, 749
- Lampeitl, H. et al. 2010, *MNRAS*, 401, 2331
- Miknaitis, G. et al. 2007, *ApJ*, 666, 674
- NASA/IPAC Extragalactic Database. 2008, *NED Velocity Correction Calculator*
- Neill, J. D., Hudson, M. J., & Conley, A. 2007, *ApJ*, 661, L123
- Page, L. et al. 2003, *ApJS*, 148, 233
- Patiri, S. G., Betancort-Rijo, J. E., Prada, F., Klypin, A., & Gottlöber, S. 2006, *MNRAS*, 369, 335
- Percival, W. J., Cole, S., Eisenstein, D. J., Nichol, R. C., Peacock, J. A., Pope, A. C., & Szalay, A. S. 2007, *MNRAS*, 381, 1053
- Percival, W. J. et al. 2010, *MNRAS*, 401, 2148
- Perlmutter, S. et al. 1999, *ApJ*, 517, 565
- Perlmutter, S., & Schmidt, B. P. 2003, in *Lecture Notes in Physics*, Berlin Springer Verlag, Vol. 598, *Supernovae and Gamma-Ray Bursters*, ed. K. Weiler, 195–217
- Pyne, T., & Birkinshaw, M. 1996, *ApJ*, 458, 46
- Riess, A. G. et al. 1998, *AJ*, 116, 1009
- . 1999, *AJ*, 117, 707
- . 2007, *ApJ*, 659, 98
- . 2004, *ApJ*, 607, 665
- Sako, M. et al. 2008, *AJ*, 135, 348
- Sasaki, M. 1987, *MNRAS*, 228, 653
- Schmidt, B. P. et al. 1998, *ApJ*, 507, 46
- Sinclair, B., Davis, T., & Haugbølle, T. 2010, *MNRAS*
- Sollerman, J. et al. 2009, *ApJ*, 703, 1374
- Spergel, D. N. et al. 2006, *ArXiv Astrophysics e-prints*
- Springel, V. 2005, *MNRAS*, 364, 1105
- Tegmark, M. et al. 2006, *Phys. Rev. D*, 74, 123507
- Vanderveld, R. A. 2008, *ApJ*, 689, 49
- Watkins, R., Feldman, H. A., & Hudson, M. J. 2009, *MNRAS*, 392, 743
- Wood-Vasey, W. M. et al. 2007, *ApJ*, 666, 694
- York, D. G. et al. 2000, *AJ*, 120, 1579
- Zehavi, I., Riess, A. G., Kirshner, R. P., & Dekel, A. 1998, *ApJ*, 503, 483
- Zheng, C. et al. 2008, *AJ*, 135, 1766
- Zibin, J. P., Moss, A., & Scott, D. 2008, *Physical Review Letters*, 101, 251303